# GRAVITATIONAL COLLAPSE AND STAR FORMATION IN LOGOTROPIC AND NON-ISOTHERMAL SPHERES

Dean E. McLaughlin and Ralph E. Pudritz
Department of Physics and Astronomy, McMaster University
Hamilton, Ontario L8S 4M1, Canada
dean@physics.mcmaster.ca, pudritz@physics.mcmaster.ca

## ABSTRACT

We present semi-analytical similarity solutions for the inside-out, expansion-wave collapse of initially virialized gas clouds with non-isothermal equations of state. Results are given for the family of negative-index polytropes ($P \propto \rho^{\gamma}$, $\gamma \leq 1$), but we focus especially on the so-called logotrope, $P/P_c = 1 + A\ \ln(\rho/\rho_c)$. In a separate paper, we have shown this to be the best available phenomenological description of the internal structure and average properties of molecular clouds and dense clumps of both high and low mass. The formalism and interpretation of the present theory are extensions of those in Shu's (1977) standard model for accretion in self-gravitating isothermal spheres: a collapse front moves outwards into a cloud at rest, and the gas behind it falls back to a collapsed core, or protostar. The infalling material eventually enters free-fall, so that the density profiles and velocity fields have the same shape ($\rho \propto r^{-3/2}$ and $-v \propto r^{-1/2}$) at small radii in logotropic and isothermal spheres both. However, several differences arise from the introduction of a new equation of state. The accretion rate onto a protostar is not constant in a logotrope, but grows as $\dot{M} \propto t^3$ during the expansion wave. Thus, the formation time for a star of mass $M$ scales as $M^{1/4}$; low-mass stars are accreted over longer times, and high-mass stars over shorter times, than expected in isothermal clouds. This result has implications for the form and origin of the stellar IMF. In addition, the gas density behind an expansion wave increases with time in our theory, but would decrease in an isothermal sphere. The infall velocities also grow, but at an initially much slower rate than found in an isothermal collapse. These results apply to low- and high-mass star formation alike. We briefly discuss how they lead to older inferred collapse ages for Class 0 protostars in general, and for the Bok globule B335 in particular.

*To appear in The Astrophysical Journal*

## 1. Introduction

One of the cornerstones in any theory of star formation has to be a correct description of the gravitational collapse of gaseous clouds. The pioneering studies of Bodenheimer & Sweigart

(1968), Larson (1969), and Penston (1969) gave numerical integrations of the isothermal collapse of uniform-density spheres, and Larson and Penston both went so far as to derive semi-analytical similarity solutions (descriptions of a fluid flow in which the densities and velocities approach invariant forms) for the evolution of their spheres. In a seminal paper which defined the current paradigm for "inside-out" collapse and low-mass star formation, Shu (1977) derived a different, one-parameter family of similarity solutions for the isothermal problem. Hunter (1977) found still more, and Whitworth & Summers (1985) finally pointed out that there is in fact a two-dimensional continuum of such solutions. Common to all of these is the eventual formation of a central point mass which subsequently grows as the cloud continues to fall onto it. This *core* is naturally identified as a protostar (or star and disk).

One of Shu's (1977) solutions in particular — the so-called expansion wave — has played a central role in the development of the standard theory of star formation, as reviewed, for example, by Shu, Adams, & Lizano (1987). In part, this is because of the simple and intuitive nature of the expansion wave, and because it lends itself well to the (perturbative) inclusion of rotation (Tereby, Shu, & Cassen 1984) and mean magnetic fields (Galli & Shu 1993a, b) in isothermal clouds. In addition, however, it is physically relevant because it describes the relatively gentle collapse, from the center on out, of a sphere which is initially in virial equilibrium. As we discuss shortly, the idea that pre-collapse interstellar clouds are in equilibrium configurations is one which meshes with a variety of observations. There are contrary arguments (e.g., Bonnell, Bate, & Price 1996) that star-forming clouds should collapse from non-equilibrium, or even near-uniform conditions; but this is a violent process (the flow of Larson [1969] and Penston [1969] is everywhere highly supersonic) which would give rise to strong kinematic signatures that have never been observed. Rather, the most convincing claim to a direct detection of collapse has been made for the Bok globule B335, where molecular line profiles are consistent with the more moderate velocity field expected for an expansion wave (Zhou 1992; Zhou et al. 1993).

The standard theory has its difficulties, however. For instance, Shu's (1977) model describes the collapse of highly unstable, *singular* isothermal spheres, and is not necessarily applicable to more realistic clouds with finite central densities (such as the marginally stable Bonnor-Ebert sphere: Hunter 1977; Foster & Chevalier 1993). As another example, an isothermal expansion wave leads to a time-invariant protostellar accretion rate, $\dot{M} = 0.975\sigma^3/G$, which appears to be inconsistent with the observed luminosities of young stellar objects in the Taurus-Auriga star-forming region specifically (e.g., Kenyon et al. 1994). But most important is the fact that an isothermal equation of state, while a natural and instructive first approximation, is ultimately incompatible with observations of both giant molecular clouds (GMCs) and the subcondensations, the dense clumps where stars are ultimately born, within them.

As suggested above, GMC complexes, and individual clumps, are well described by models of (magnetic) virial-equilibrium spheres which are "truncated" by a constant surface pressure exerted by a diffuse external medium (e.g., Myers & Goodman 1988; Bertoldi & McKee 1992; Elmegreen 1989; McLaughlin & Pudritz 1996). (The dense clumps are often referred to as cores, but here we

reserve that term for the central point mass, or protostar, which develops in a collapsing sphere.) The virial balance relies on superthermal random velocities which *increase outwards* within any given clump. The nonthermal component $\sigma_{\rm NT}$ of the total velocity dispersion (linewidth) is larger in higher-mass clumps (Caselli & Myers 1995), but is present at even the smallest observed radii in low-mass clumps as well (Fuller & Myers 1992). Indeed, $\sigma_{\rm NT}$ grows more rapidly with increasing radius in low-mass clumps than in high-mass ones, and *no interstellar cloud obeys an isothermal equation of state.*

The first attempts to model the nonthermal linewidths (e.g., Myers & Fuller 1992; Lizano & Shu 1989) tended to focus on the fact that $\sigma_{\rm NT}$ is small in low-mass clumps. Myers & Fuller, in particular, construct equilibrium, self-gravitating spheres from a gas equation of state (EOS) which is explicitly isothermal at small radii in a cloud, and becomes progressively "softer" ($P$ depends less than linearly on $\rho$, so that $\sigma^2 = P/\rho$ increases with decreasing density) further out. Because the clumps in GMCs can be viewed as pressure-truncated spheroids, with truncation at a smaller radius corresponding to a lower mass, this approach effectively ensures that the low-mass clumps are still treated as (very nearly) isothermal spheres. Any consequences which the nonthermal support might have for collapse and star formation are then largely confined to the high-mass regime. For example, Myers & Fuller (1992) estimate the formation times of stars in their model, and conclude that high-mass stars are accreted relatively faster than they would be under an isothermal EOS, while low-mass stars grow at roughly the same rate.

By contrast, McLaughlin & Pudritz (1996=MP96) have adopted a phenomenological, *logotropic* EOS — $P/P_c = 1 + A\ \ln(\rho/\rho_c)$ — for molecular clouds and clumps. This EOS provides a unified treatment of low- and high-mass clumps and entire GMCs. It can account quantitatively for (1) the global size-linewidth and mass-radius relations (e.g., Larson 1981) *between* cloud complexes; (2) the typical mass and density contrasts between GMCs and the clumps within them; and (3) the observed dependence of linewidth on radius *inside* dense clumps of any mass. Moreover, the form of the EOS itself is never close, even on small spatial scales or in low-mass clouds, to the isothermal $P \propto \rho$. The details of *both* low- *and* high-mass star formation in a logotrope will therefore differ from the standard results for isothermal collapse. (It should be noted that our logotrope is different from that introduced by Lizano & Shu [1989], which essentially has $P \sim \rho + \ln\rho$, and cannot account for all three of the properties of interstellar clouds listed here.)

In this paper, then, we derive semi-analytical similarity solutions for the collapse of nonmagnetic, non-rotating gas spheres with softer-than-isothermal equations of state. We concentrate on the case of a logotropic EOS as the most self-consistent description of the ubiquitous turbulence in interstellar clouds; but in a pair of Appendices, results are also given for the more general family of negative-index polytropes ($P \propto \rho^\gamma$, with $0 < \gamma \leq 1$). (Although the self-similar collapse of polytropes has previously been investigated by, e.g., Suto & Silk [1988], we also briefly discuss the accretion rates and star formation timescales in such spheres.)

Section 2 begins with a brief summary of the equilibrium structure of a logotrope (MP96),

and then goes on to an analysis of its collapse. Our development owes much to the physical discussion of Shu (1977): we first find a class of collapse solutions for singular, $\rho \propto r^{-1}$ spheres which are very accurate approximations to more realistic, non-singular logotropes, and then focus on the inside-out, expansion-wave collapse of an initially virialized cloud. Two main features are a post-collapse density profile and velocity field which have the same free-fall shape ($\rho \propto r^{-3/2}$ and $-u \propto r^{-1/2}$ at small radii) found for an isothermal expansion wave, *but* a rate of accretion onto the collapsed core which is no longer constant in time; rather, $\dot{M} \propto t^3$ here. These results allow for an evaluation, in §3, of the formation times for stars of various masses. High-mass stars will be accreted more rapidly in a logotrope than in an isothermal sphere, but a low-mass star in a logotrope will appear later than a star of the same mass would in an isothermal sphere. This "squeezing" of formation timescales, which we estimate to be typically of order $1 - 3 \times 10^6$ yr, should have important implications for the origin and shape of the stellar IMF. In §4 we consider the collapse of a 1 $M_\odot$ logotrope specifically, and briefly discuss relevant observations of two young stellar objects, NGC 2071 and B335. We conclude that the age of B335 is probably greater than $10^6$ yr, an order of magnitude older than suggested by the application of isothermal collapse models. Since B335 is one of the family of the youngest known, "Class 0" protostars (André, Ward-Thompson, & Barsony 1993), these objects might generally be rather older than is currently believed.

## 2. Similarity Solutions

### 2.1. The Logotrope

Our logotropic EOS (MP96) is

$$\frac{P}{P_c} = 1 + A \ln\left(\frac{\rho}{\rho_c}\right) \ , \tag{2.1}$$

where $P_c$ and $\rho_c$ are the central pressure and density in a cloud, and $A$ is essentially a free parameter. The total velocity dispersion $\sigma^2 = P/\rho$ increases outwards from $r = 0$ until it reaches a maximum at some large radius, beyond which it decreases somewhat. Since linewidths are essentially purely thermal on the smallest scales in real interstellar clouds, and are also observed to increase with radius (e.g., Fuller & Myers 1992; Caselli & Myers 1995), the central velocity dispersion in a logotrope is identified with the thermal value: $\sigma_c^2 \equiv P_c/\rho_c = kT/\mu m_H$. Once a value of $A$ is specified, the EOS (2.1) can be used to integrate a Lane-Emden type of equation for a self-gravitating, virialized gas sphere. This then allows for a quantitative comparison of the *internal* $\sigma$ vs. $r$ profiles of real and model clouds. Good agreement with data on GMC clumps, of low and high mass alike, is obtained for $A \simeq 0.2 \pm 0.02$.

These points are discussed in more detail in MP96. Starting from the premise that interstellar clouds are pressure-truncated — their boundaries defined by a surface pressure $P_s$ due to a more diffuse, surrounding medium — that paper develops expressions for the masses and densities of

virial-equilibrium gas spheres with arbitrary equations of state. Quite general arguments then imply that GMCs, and the *largest* clumps within them, are all at or near their critical masses: if they were any more massive, given their temperatures, surface pressures, and magnetic field strengths, they would be unstable to radial perturbations (see also McKee 1989; Bertoldi & McKee 1992). Although this conclusion is independent of the exact form of the gas EOS, not all equations of state provide for such a critical mass. For example, the family of negative-index polytropes (in which $P \propto \rho^{\gamma}$, with $\gamma < 1$) also have velocity dispersions that increase with radius, but are *always stable* against radial perturbations in the analysis of MP96. Put another way, and independently of any stability analysis, such polytropes cannot simultaneously account for the internal structure of molecular clumps and the global properties (Larson's [1981] laws: $M \propto R^2$ and $\sigma_{\rm ave} \propto R^{1/2}$) of GMCs; the logotrope is the simplest EOS for which this is possible.

The critical mass of an $A = 0.2$ logotrope is given by equation (2.11) of MP96:

$$M_{\rm crit} = \frac{250}{\alpha^{3/2}}\ M_{\odot}\ \left(\frac{T}{10\ {\rm K}}\right)^2 \left(\frac{P_s}{1.3\times 10^5\ k\ {\rm cm}^{-3}\ {\rm K}}\right)^{-1/2}\quad , \tag{2.2}$$

where we have explicitly used the fact that $\sigma_c^2 = kT/\mu m_H$, and set the mean molecular weight to $\mu = 2.33$. The constant $\alpha$ here depends on the strength of any mean magnetic field threading the cloud. If there is equipartition between kinetic and mean magnetic energies, then $\alpha \approx 1$; in the absence of any mean field at all, $\alpha = 35/18$ for the logotrope and $M_{\rm crit} \simeq 92 M_{\odot}$ for this temperature and surface pressure. A smaller value of $A$ results in a larger critical mass: for example, $A = 0.18$ would raise $M_{\rm crit}$ by a factor of about 2.5. MP96 also derive the mean density of a critical-mass logotrope:

$$\rho_{\rm ave,crit} = 1.31\times 10^{-20}\ {\rm g\ cm}^{-3}\ \left(\frac{T}{10\ {\rm K}}\right)^{-1} \left(\frac{P_s}{1.3\times 10^5\ k\ {\rm cm}^{-3}\ {\rm K}}\right)\quad . \tag{2.3}$$

The fiducial $P_s$ chosen here is appropriate for dense clumps embedded in self-gravitating GMCs, which amplify the pressure of the hot ISM by about an order of magnitude (Elmegreen 1989; Bertoldi & McKee 1992); it is also similar to the value adopted by Shu (1977) in his study of isothermal collapse. It is significant that the logotropic $M_{\rm crit}$ is vastly greater than the $\sim 1 M_{\odot}$ mass of a critical, $T = 10$ K isothermal sphere under the same surface pressure. This is part of what makes our model more consistent with observations of the ISM, and in particular with the arguments, mentioned above, that only the largest clumps in GMCs are at their critical mass, with smaller ones being in a stable virial equilibrium.

Because we are dealing with pressure-truncated spheres, a cloud's mass can be viewed as being set by the dimensionless "truncation radius" $R/r_0$ (where $r_0 \equiv 3\sigma_c/[4\pi G\rho_c]^{1/2}$) at which the internal pressure equals that of an ambient medium. That is, there is an EOS-dependent $R/r_0$ which corresponds to a critical-mass cloud; any smaller $R/r_0$ is equivalent to a unique $M/M_{\rm crit} < 1$. Indeed, $R/r_0$, along with a surface pressure $P_s$ and kinetic temperature $T$, determines all the properties of a cloud (see Appendix A of MP96). An example of this is given in Table 1, where we

list the center-to-edge density and pressure contrasts, mean density, and mass-averaged linewidth (thermal plus nonthermal: $\sigma^2_{\rm ave} = P_{\rm ave}/\rho_{\rm ave}$) for logotropes with $A = 0.2$. The absolute values of the masses and free-fall times there ($\bar{t}_{\rm ff} = [3\pi/32G\rho_{\rm ave}]^{1/2}$) apply to purely hydrostatic spheres with no mean magnetic fields, as these are the types of objects which our collapse calculations will directly address. If $P_s$ or $T$ is changed, the mass and mean density of the critical cloud will be affected as in equations (2.2) and (2.3). Then, because the dimensionless $R/r_0$ actually determines the mass and free-fall time relative to the critical values, these quantities will both change at every radius in Table 1, and by the same factors as in the critical cloud. In any case, it is significant that the total linewidth $\sigma_{\rm ave}$ is generally larger in bigger clouds. Lower-mass objects are supported to a greater, *but not complete* extent by thermal motions.

Figure 1 shows the density profile of a critical-mass logotrope, and compares it with that of a critical-mass, or Bonnor-Ebert, isothermal sphere (Bonnor 1956; Ebert 1955; McCrea 1957). The structure of less massive spheres can also be derived from this diagram; for example, the $\rho$ vs. $r$ curve for a logotrope with $M/M_{\rm crit} \simeq 0.33$ is obtained by vertically shifting the curve in Fig. 1 such that $\rho/\rho_s = 1$ at $r/r_0 \simeq 9.4$ (cf. Table 1). Also shown in the Figure, as broken lines, are the analytical singular solution to the equation of hydrostatic equilibrium for a self-gravitating logotrope (MP96),

$$\rho(r) = (AP_c/2\pi G)^{1/2}\ r^{-1}\ , \tag{2.4}$$

and the singular solution $\rho(r) = (\sigma_c^2/2\pi G)\ r^{-2}$ for an isothermal sphere. Equation (2.4) closely approximates the bounded logotrope (finite central density; solid line) at all $r/r_0 \gtrsim 0.4$, and thus adequately describes the structure even of stable low-mass spheres. On the other hand, the singular isothermal sphere bears very little relation to the Bonnor-Ebert configuration. (The logotropic prediction $\rho \propto r^{-1}$ is one with some observational support. This is discussed in MP96; here we note only that an observed column density profile $N \propto r^{-1}$, which is not uncommon, does *not* necessarily imply $\rho \propto r^{-2}$.)

Since a low-mass clump (say, $M_{\rm tot} \sim 1 M_\odot$) is expected to be globally stable against radial perturbations, how does it come to collapse and form a star? When magnetic fields are present, ambipolar diffusion should induce a slow contraction of the clump, during which its initial (time $t = -\infty$) central concentration will be enhanced and its density profile brought into agreement with the singular solution (2.4) over essentially all radii — a configuration that is manifestly unstable (e.g., MP96). Alternatively, in a purely hydrodynamic situation, collapse could be initiated by the growth of a local density fluctuation; or the clump could be put out of equilibrium by the accretion of mass from the surrounding medium. The time at which a cloud becomes singular is labelled $t = 0$, and corresponds to the formation of a central point mass (or core; physically, a protostar and disk). Following Shu (1977), it is the subsequent, $t \geq 0$ evolution of nonmagnetic spheres that we now examine in detail.

### 2.2. Fluid Equations

We begin with the usual Eulerian equations for spherically symmetric flow in a self-gravitating fluid (cf. Larson 1969; Shu 1977):

$$\begin{aligned}
\frac{\partial u}{\partial t} + u\frac{\partial u}{\partial r} + \frac{GM}{r^2} + \frac{dP}{d\rho}\frac{\partial\ \ln\rho}{\partial r} &= 0 && (2.5)\\
\frac{\partial M}{\partial t} + 4\pi r^2 \rho u &= 0 && (2.6)\\
\frac{\partial M}{\partial r} - 4\pi r^2 \rho &= 0\ , && (2.7)
\end{aligned}$$

where $M(r,t)$ is the *total* mass (including any core) inside radius $r$ at time $t$, and $u(r,t)$ is the instantaneous fluid velocity. The gas EOS influences the collapse through the pressure force $\rho^{-1}\partial P/\partial r$ in equation (2.5). For the most part, we confine our attention to the logotropic EOS (eq. [2.1]), but in Appendices A and B below we also consider the more general family of negative-index polytropes.

We define a similarity variable

$$x = \frac{r}{a_t t}\ , \tag{2.8}$$

where $a_t$ is a function of time with dimensions of velocity. Dimensionless density, velocity, and mass variables may then be set up as

$$\alpha(x) = 4\pi G t^2 \rho(r,t) \qquad v(x) = u(r,t)/a_t \qquad m(x) = GM(r,t)/a_t^3 t\ . \tag{2.9}$$

Further, because the square of the sound speed is $dP/d\rho = AP_c/\rho$ for this EOS, we are led to set

$$a_t = [AP_c(4\pi G t^2)]^{1/2}\ , \tag{2.10}$$

where $A \simeq 0.2$ for real interstellar clouds, and where the constant $P_c$ refers to the central pressure in the *initial*, pre-collapse ($t = -\infty$) cloud (as such, it reflects the constant pressure of the ambient medium, and the total mass of the cloud; see, e.g., Table 1). Ultimately, the central core mass grows as $M(0,t) \propto a_t^3 t \propto t^4$, and the accretion rate as $\dot{M}(0,t) \propto t^3$. This is in sharp contrast to an isothermal collapse, where the accretion rate is constant in time (see §3 below for further discussion). In any case, straightforward manipulation of equations (2.5) – (2.7) yields

$$\begin{aligned}
\left[(2x-v)^2 - \frac{1}{\alpha}\right]\frac{d\ \ln\alpha}{dx} &= \left[\frac{\alpha}{4} - \frac{2}{x}(2x-v)\right](2x-v) + [2(2x-v)+v] && (2.11)\\
\left[(2x-v)^2 - \frac{1}{\alpha}\right]\frac{dv}{dx} &= \left[\frac{\alpha}{4}(2x-v) - \frac{2}{\alpha x}\right](2x-v) + \left[\frac{2}{\alpha} + v(2x-v)\right] && (2.12)\\
m &= \frac{\alpha x^2}{4}(2x-v)\ . && (2.13)
\end{aligned}$$

These equations are written in a form similar to that of Shu (1977) for the isothermal sphere, which is included as a special case in the general development of Appendix A below.

There are two simple analytical solutions of equations (2.11) – (2.13). The first has a uniform density,

$$\alpha = \frac{2}{3} \qquad v = \frac{2x}{3} \qquad m = \frac{2x^3}{9} \ , \tag{2.14}$$

and is equally valid for any polytropic EOS. Of more interest is the static (singular) solution,

$$\alpha = \frac{\sqrt{2}}{x} \qquad v \equiv 0 \qquad m = \frac{x^2}{\sqrt{2}} \ . \tag{2.15}$$

This corresponds to a time-independent density profile, $\rho(r) = (AP_c/2\pi G)^{1/2}\ r^{-1}$, which is just that found (eq. [2.4]) to satisfy the equation of hydrostatic equilibrium for a self-gravitating logotrope. As discussed in §2.1, it also describes the large-radius structure of the bounded sphere — the type of cloud we expect to begin with at $t = -\infty$.

An entire class of singular solutions, valid at large radii or small (positive) times, can be found by taking $\alpha$ and $|v|$ to be much smaller than $x$ in equations (2.11) – (2.13). In this $x \rightarrow \infty$ limit, we have

$$\alpha \rightarrow \frac{C}{x} \qquad v \rightarrow -\frac{C}{2}\left(1 - \frac{2}{C^2}\right) \qquad m \rightarrow \frac{Cx^2}{2} \ . \tag{2.16}$$

For an inflow scenario ($v < 0$), the density normalization $C$ must be greater than the hydrostatic-equilibrium value $\sqrt{2}$. Each $C > \sqrt{2}$ therefore corresponds to the collapse of a logotrope which is initially just out of equilibrium, with densities (and pressures) everywhere enhanced by a factor $1 + \delta = C/\sqrt{2}$. As in the equilibrium case, the cloud starts at $t = -\infty$ with a finite central density, and $\rho$ at large radii given by equation (2.16), and then contracts to follow that singular profile everywhere by $t = 0$. These solutions are the analogues of Shu's (1977) "minus solutions without critical points" for the singular isothermal sphere — although we show in §2.3 that in our case, some of the out-of-equilibrium flows *can* pass through critical points.

Although $v$ is a finite constant at $t = 0$ here, the dimensional velocity $u \sim vt$ vanishes, and the cloud is essentially at rest at the time of core formation. This is consistent with a physical picture at $t < 0$ of quasistatic evolution towards the singular profile. As suggested above, such a slow contraction could be driven by ambipolar diffusion, and we therefore view the family of solutions (2.16) as reasonable starting points for the post-core formation evolution of a collapsing logotrope. This is the same tack taken by Shu (1977) in his treatment of the isothermal sphere, but in one important way it is perhaps better justified for our EOS. If it happens that the mean magnetic field is initially weak and unable to significantly influence the evolution of a cloud, then the assumption of a gentle approach to the singular profile, and the validity of equations (2.16) in the $t = 0$ limit of the collapse, have to be questioned

The singular isothermal sphere is a poor description of the critical-mass Bonnor-Ebert configuration, or of any less massive one (see Fig. 1). Thus, purely hydrodynamic collapse simulations of the latter clouds (e.g., Hunter 1977; Foster & Chevalier 1993) differ significantly from the results of Shu (1977). The approach to an $r^{-2}$ profile at $t = 0$ is rather violent for them,

and involves appreciable fluid velocities that invalidate the main premise ($u = 0$ at $t = 0$) of the similarity solutions discussed here and by Shu. The subsequent $t > 0$ collapse then proceeds much more rapidly than for a singular sphere, with an accretion rate that decreases over time. In our case, the logotropic singular solution ($\rho \propto r^{-1}$: eq. [2.4] and Fig. 1) *does* describe the structure of bounded clouds of any interesting mass. The adjustment to a fully singular profile at $t = 0$ should then be a relatively easy one, and it is reasonable to expect that equations (2.16) adequately describe any collapsing logotrope at the point of core formation. This argument is consistent with numerical simulations (Foster & Chevalier 1993) for the collapse of a bounded isothermal sphere whose central concentration is ~70 times that of the Bonnor-Ebert value. Although such a cloud is highly unstable, it is well approximated at large radii by the singular isothermal sphere, and its accretion rate quickly approaches the constant value predicted by Shu (1977).

Turning now to the opposite limit of small radii, $x \to 0$, we have that $|v|,\ \alpha \to \infty$ for collapse, and thus

$$\alpha \to 4\left(\frac{m_0}{2x^3}\right)^{1/2} \qquad v \to -\left(\frac{2m_0}{x}\right)^{1/2} \qquad m \to m_0\ , \tag{2.17}$$

where the reduced mass $m_0$ of the collapsed core also serves to fix the accretion rate onto the core ($\dot{M}_0 \propto m_0 t^3$ by eq. [2.9]; see also §3 below). The effects of shocks (e.g., Tsai & Hsu 1995) and radiation pressure (for massive stars; Jijina & Adams 1996) will invalidate this solution at very small $x$, but should not affect our discussion of the area external to such disturbed regions, nor the value of $m_0$ itself.

The $x^{-3/2}$ and $x^{-1/2}$ scalings of $\alpha$ and $v$ here are identical to the corresponding results for the isothermal sphere (Shu 1977), or any other polytrope with $0 < \gamma < 1$ (Appendix A). This reflects the fact that the ratio of gravitational and pressure forces,

$$\frac{GM/r^2}{\rho^{-1}dP/dr} = \frac{m\alpha}{x}\left(\frac{d\ \ln\alpha}{d\ \ln x}\right)^{-1} \to -\frac{4\sqrt{2}}{3}\,\frac{m_0^{3/2}}{x^{5/2}}\ , \tag{2.18}$$

increases without limit as $x \to 0$, and the gas at very small radii approaches the core in free-fall. At any fixed time $t > 0$, the dimensional velocity field near the center therefore tends to $u = (2GM_0/r)^{1/2}$, and the density profile to

$$\rho(r) = \frac{\dot{M}}{4\pi r^2 u} = \frac{\dot{M}}{4\pi(2GM_0)^{1/2}}\ r^{-3/2}\ , \tag{2.19}$$

which is equivalent to equation (2.17) for a spatially invariant accretion rate $\dot{M}$. When written this way, the effects of the gas EOS are completely contained in the values of $\dot{M}$ and $M_0$ at a given time; at least in the absence of rotation and magnetic fields, *observations of the shape of the density profiles or velocity fields in the central regions of a collapsing cloud are insufficient to constrain the underlying equation of state*. Any data which favor an $r^{-3/2}$ density profile in such objects (e.g., Butner et al. 1990, 1991) are qualitatively consistent with both the logotropic hypothesis and the isothermal one (quantitatively, however, the different accretion *histories* in the two models may well allow for an empirical discrimination between them; see §4 below). By

the same token, observations which suggest a different structure (e.g., André et al. 1993) are a challenge to both scenarios.

A full similarity solution for the collapse of overdense clouds, over all times $t \geq 0$ and all radii $r \geq 0$, begins at large $x$ as in equation (2.16), and eventually tends to the form (2.17) at small $x$. As such, there is a one-to-one relation between $C$ and $m_0$. This is obtained by numerical integration of equations (2.11) and (2.12), and is laid out in Table 2. Evidently, the larger the overdensity $C/\sqrt{2}$, the larger is the reduced core mass $m_0$, and the faster the accretion rate. The limit $C \to \sqrt{2}$ refers to the collapse of a logotrope which is initially arbitrarily close to hydrostatic equilibrium. In this situation — which is the parallel of Shu's (1977) expansion-wave solution for the singular isothermal sphere — a collapse front propagates outwards in a cloud at rest, with the material behind it falling away to the center.

### 2.3. Critical Points and the Expansion Wave

A look at equations (2.11) and (2.12) shows that when a collapse solution passes through a point $x_* \geq 0$ which has

$$2x_* - v_* - \alpha_*^{-1/2} = 0 \ , \tag{2.20}$$

the derivatives $d\alpha/dx$ and $dv/dx$ will be undefined unless the quantities on the right-hand side of the fluid equations also vanish there. Any valid flow must therefore satisfy

$$\frac{\alpha_*^{1/2}}{4} + \frac{1}{\alpha_*^{1/2}} - \frac{2}{x_* \alpha_*} + 2x_* = 0 \tag{2.21}$$

at such *critical points*. Mathematically, the $\alpha(x)$ and $v(x)$ which everywhere satisfy these two relations would present a third analytical similarity solution for our problem; but it is one which relies on a rather special interplay between the fluid variables, and one which we therefore neglect. Instead, physical flows must either avoid the line of critical points (or singular points, or sonic points) defined by equations (2.20) and (2.21), or else pass right through it.

Whitworth & Summers (1985) elaborate on the topology of critical points and the implications for a self-similar, isothermal collapse, and we refer the interested reader to that paper for an excellent discussion of such issues. Here we note that, for any gas EOS, a linearization of the fluid equations in the neighborhood of any critical point $x_*$ leads to three pairs of eigenvalues for the slopes $d\alpha/dx$ and $dv/dx$ there, and hence to three eigensolutions for $\alpha(x)$ and $v(x)$. One of these is physically inadmissible but the other two, corresponding to the "minus" and "plus" solutions of Shu (1977), have the velocity either decreasing or increasing towards smaller $x$. They are described quantitatively, for the logotrope and for negative-index polytropes, in Appendix B.

It is the minus solutions, for which $v \to -\infty$ as $x \to 0$, that are of most interest in the collapse context. The velocity fields for some representative examples are shown as the solid lines in Fig. 2. Also shown there are the locus of critical points (dash-dot line) defined above, and a few plus

solutions (dashed lines). We will not discuss the plus solutions, other than to say that (1) their time-reversed counterparts could be of interest in a wind problem, and (2) in the limit $x \to \infty$, they have $\alpha \sim x^{-4}$, $v \sim x^2$, and $\alpha v^2 = \rho u^2/AP_c = 2$.

Our Fig. 2 should be compared to that of Shu (1977). The heavy black line here is the expansion-wave solution mentioned above. It passes through the critical point $x_* = 0.02439$, and is the limit of two different sequences of minus solutions. Those which pass through critical points $x_* < 0.02439$, to the left of the expansion wave, go on to a stagnation point ($v = 0$) at some finite $x$, beyond which there is outflow. These solutions are therefore of no interest to us, although they might be useful in modelling the effects of accretion shocks (see Tsai & Hsu 1995). If they were to be simply truncated at the point where $v = 0$, they would have vanishingly small spatial extent at $t = 0$, which is unacceptable; and, as in the isothermal case, the static solution (eq. [2.15]) cannot be used to continue such flows to infinite $x$ because there is a mismatch in the densities at the stagnation point. The densities and velocities still follow the power laws of equation (2.17) at small $x$, though, with a core mass $m_0$ that is uniquely defined by the location of the critical point $x_*$ and is always less than the expansion-wave value.

Fundamentally, the expansion wave is identified as an extreme member of this family of solutions because its stagnation point is also a critical point, $x_* = x_{\rm ew}$. In this case (see Appendix B),

$$x_{\rm ew} = \frac{1}{4\sqrt{2}} \quad \Rightarrow \quad \alpha_{\rm ew} = 8 \qquad v_{\rm ew} = 0 \qquad m_{\rm ew} = \frac{1}{32\sqrt{2}} \qquad m_0 = 6.67 \times 10^{-4}\ . \tag{2.22}$$

These results do agree with the static cloud profile (2.15) at $x = x_{\rm ew}$, and the core mass $m_0$ corresponds to that in the $C \to \sqrt{2}$ collapse (cf. Table 2 above), so an extension to arbitrarily large $x$ is obtained by simply joining the two solutions in the obvious way. In fact, the logotropic expansion wave comes into $x_{\rm ew}$ from the left with velocity and density derivatives, $(dv/dx)_{x_{\rm ew}} = 0$ and $(d\alpha/dx)_{x_{\rm ew}} = -1/32\sqrt{2}$, which also agree with those of the static profile, i.e., the flow is *continuous* at $x_{\rm ew}$. This is the case for any polytropic EOS with $\gamma \leq 3/5$, but when $\gamma > 3/5$ (including the isothermal $\gamma = 1$) there is a discontinuity at the matching point (see Appendix B).

Physically, as discussed above and by Shu (1977), an expansion wave corresponds to the inside-out collapse of a cloud which is in hydrostatic equilibrium at the moment $t = 0$ of core formation. At any point in time (before the expansion wave reaches the initial cloud surface), a total reduced mass of $m_{\rm ew}$ is involved in the collapse, with a small fraction $m_0/m_{\rm ew} \simeq 0.03$ of that having already fallen onto the central core. It may also be shown (for any gas EOS) that since the point $x_{\rm ew}$ is fixed in similarity space, the wave propagates into the cloud always at the *local* speed of sound, $(dP/d\rho)^{1/2}$.

However, the logotrope differs from the isothermal sphere, in that its expansion wave passes through two critical points: $x_* = 0.02439$ and $x_* = x_{\rm ew}$. (For an isothermal EOS, the expansion-wave $v$ is just tangent to the locus of critical points at $x_{\rm ew}$, and does not cross it anywhere.) It is the presence of these two distinct critical points, *both* with $v_* \leq 0$, which also

marks the expansion-wave flow as the limit of a second sequence of minus solutions, namely, the out-of-equilibrium collapse profiles encountered in §2.1 (eq. [2.16]). Several of these are drawn on Fig. 2, to the right of the expansion wave, and labelled by their density normalizations $C$. Evidently, for $C$ close enough to the hydrostatic-equilibrium value of $\sqrt{2}$, such solutions — which have $v < 0$ everywhere — also pass through two critical points. This is again in contrast to the isothermal situation, in which all out-of-equilibrium collapses are free of critical points. On some level, however, this is just a mathematical issue; there is nothing intrinsically unphysical or artificial about flow through a critical point.[1]

## 3. Accretion Timescales

Once numerical solutions to the self-similar fluid equations have been obtained, and the reduced mass $m_0$ found for any minus solution, we have a description of the growth of the central core in a collapsing cloud. The formation times for stars of various masses can then be computed. Again, we focus on the results for logotropic expansion waves in this Section. Generalizations to out-of-equilibrium collapses, and to more general polytropic equations of state, are fairly straightforward (cf. Appendix A).

From equations (2.13) for the dimensionless mass $m$ and (2.17) for our similarity solutions at small radii, the central core mass is given by

$$\begin{aligned} M(0,t) \equiv M_0 &= [AP_c(4\pi G)]^{3/2}\ \frac{m_0 t^4}{G} \\ &= A^{3/2}\left(\frac{3\pi^2}{8}\frac{\rho_c}{\rho_{\rm ave}}\right)^{3/2} \frac{t^4}{\bar{t}_{\rm ff}^3}\ \frac{m_0\sigma_c^3}{G}\ . \end{aligned} \tag{3.1}$$

Here $\rho_c$ and $\rho_{\rm ave}$ are the central and mean densities of the initial ($t = -\infty$) cloud; $\bar{t}_{\rm ff}$ is its mean free-fall time, $(3\pi/32G\rho_{\rm ave})^{1/2}$; and it will be recalled that $A = 0.2$ in the logotropic EOS is most appropriate for real molecular clumps and GMCs. The ratio $\rho_c/\rho_{\rm ave}$ and the free-fall time are referred to their values in the non-singular cloud because these are then related to the surface pressure, kinetic temperature, and total mass (by, e.g., Table 1 above), which fundamentally control the collapse. As also discussed in §2.1, $\sigma_c$ is just the thermal linewidth, $(kT/\mu m_H)^{1/2}$.

[1]Fig. 2 shows that the $C \simeq 1.4245$ collapse just brushes the locus of critical points at a single $x_* \simeq 0.1034$. Solutions for $C > 1.4245$ then bypass all critical points, while those with $\sqrt{2} < C \leq 1.4245$ encounter two critical points (one less than 0.1034, and one greater). In the language of Whitworth & Summers (1985), the points with $x_* < 0.1034$ are *saddles*; those with $x_* > 0.1034$, *nodes*; and $x_* = 0.1034$ itself is degenerate. (The direction of stable numerical integration is away from a saddle, but towards a node; and only a pure plus or minus solution can pass through a saddle, while any function can cross a node.) The degeneracy moves towards larger $x$ for increasing polytropic index $\gamma$, and occurs at $x_* = 1 = x_{\rm ew}$ in the limit $\gamma = 1$. This is why the isothermal expansion wave is only ever tangent to the line of critical points, and why the overdense collapse solutions ($C > 2$ in that case) do not involve critical points at all.

The logotropic EOS already accounts for the presence of turbulence in the initial cloud, and $\sigma_c$ is therefore *not* to be interpreted as the type of "effective" sound speed discussed by, e.g., Shu et al. 1987. The accretion rate is therefore

$$\dot{M}_0 \;=\; 4A^{3/2}\left(\frac{3\pi^2}{8}\frac{\rho_c}{\rho_{\rm ave}}\right)^{3/2}\left(\frac{t}{\bar{t}_{\rm ff}}\right)^3\frac{m_0\sigma_c^3}{G} \;=\; 4\langle\dot{M}_0\rangle\ , \tag{3.2}$$

where $\langle\dot{M}_0\rangle$ is the mean rate $M_0/t$. As we discuss further in §4, the time dependence of this quantity is the most important consequence of the move away from an isothermal EOS, which gives a constant $\dot{M}_0 = \langle\dot{M}_0\rangle = 0.975\sigma_c^3/G$ for the expansion wave (Shu 1977; also Appendix A below). $\langle\dot{M}_0\rangle$ increases with time in our case, and in any negative-index polytrope, because density profiles shallower than $r^{-2}$ put more mass at larger radii in a cloud.

Now consider a pressure-truncated logotrope which is in hydrostatic equilibrium, and large enough that the singular $r^{-1}$ density profile holds at the edge of the cloud. The analysis of MP96 gives the total mass and radius as

$$M_{\rm tot} = \frac{(3A)^{3/2}}{\pi}\left(\frac{\rho_c}{\rho_{\rm ave}}\right)^{3/2}\bar{t}_{\rm ff}\ \frac{\sigma_c^3}{G} \tag{3.3}$$

and

$$R = \frac{2(3A)^{1/2}}{\pi}\left(\frac{\rho_c}{\rho_{\rm ave}}\right)^{1/2}\bar{t}_{\rm ff}\ \sigma_c\ . \tag{3.4}$$

Apart from corrections for the presence of mean magnetic fields (MP96), these expressions are valid for a cloud of any mass as long as the $r^{-1}$ profile is achieved inside it. In turn, as we have seen (cf. Fig. 1), this occurs for the full range of clump masses — from $< 1$ to several hundred $M_\odot$ — seen in GMCs. As the expansion wave moves outwards in a logotrope, equations (3.1) and (3.3) give for the fractional core mass (independently of the EOS parameter $A$)

$$\frac{M_0}{M_{\rm tot}} = \frac{\pi^4}{16\sqrt{2}}\left(\frac{t}{\bar{t}_{\rm ff}}\right)^4\ m_0\ , \tag{3.5}$$

where, again, $m_0 = 6.67\times 10^{-4}$. Also, the definition of $a_t$ (eq. [2.10]) locates the boundary of the cloud in similarity space:

$$X \equiv \frac{R}{a_t t} = \frac{4\sqrt{2}}{\pi^2}\left(\frac{t}{\bar{t}_{\rm ff}}\right)^{-2}\ . \tag{3.6}$$

Since the head of the expansion wave is at $x_{\rm ew} = 1/4\sqrt{2}$ for the logotrope, equation (3.6) shows that it reaches the surface of a collapsing cloud (of any mass) at

$$t_{\rm ew} = \frac{4\sqrt{2}}{\pi}\ \bar{t}_{\rm ff}\ , \tag{3.7}$$

i.e., after $\simeq$1.80 initial free-fall times. At that point, equation (3.5) (or the ratio $m_0/m_{\rm ew}$ from eq. [2.22]) gives $M_0/M_{\rm tot} \simeq 0.03$. If the similarity solution continues to hold after this time, then

the entire cloud will be accreted onto the core (i.e., $M_0/M_{\rm tot} = 1$ in eq. [3.5]) by

$$t_{\rm end} = \frac{2}{\pi}\left(\frac{\sqrt{2}}{m_0}\right)^{1/4} \bar{t}_{\rm ff} \simeq 4.32\ \bar{t}_{\rm ff}\ . \tag{3.8}$$

The inside-out collapse described by the expansion-wave solution is the gentlest possible, and therefore also the slowest. Solutions of the type (2.16), with $C > \sqrt{2}$ for a sphere which is initially denser than allowed for equilibrium, lead to faster accretion because of an increase in $m_0$ (Table 2) and because of an increase in the total mass (3.3), by a factor $(C/\sqrt{2})^{3/2}$ (see Appendix A).

Realistically, once the expansion wave reaches the boundary of a cloud which is under a constant surface pressure, it should be reflected and driven back into the cloud as a compression wave. Thus, our similarity solution cannot be exact beyond $t_{\rm ew}$, and the resulting estimate of $t_{\rm end}$ might be something of an upper limit. However, it does seem likely that more than one additional free-fall time is required to complete the collapse after $t_{\rm ew}$, because the accreting gas is in free is in free-fall only deep inside the expansion wave (at $x < 0.1x_{\rm ew}$; cf. eq. [2.18]). In the absence of detailed numerical simulations, then, the most secure conclusion is that the collapse of a (near-)equilibrium logotrope lasts for $t_{\rm end} > t_{\rm ew} + \bar{t}_{\rm ff} \gtrsim 3\bar{t}_{\rm ff}$ after core formation. However, if the isothermal sphere is any guide, then the simulations of Boss & Black (1982) and Foster & Chevalier (1993) suggest that the correct time to $M_0 = M_{\rm tot}$ for a logotrope may in fact be fairly close to our equation (3.8): The core in Boss & Black's numerical collapse of a non-rotating, equilibrium singular sphere grows at roughly the expansion-wave rate even after $t_{\rm ew}$; and the results of our Appendix A can be used to compute a $t_{\rm end}$ which is only ∼20% longer than the total accretion time in Foster & Chevalier's "$\xi_{\rm max} = 40$" run for a cloud that is overdense by 10% and has high but finite concentration at $t = -\infty$.

Figure 3 shows the density profile and velocity field, in similarity space, for a full expansion-wave solution. The thick black lines lie inside the head of the expansion wave, which is at $x_{\rm ew} \simeq 0.177$. At larger $x$, the density profile is given by the hydrostatic singular solution $\alpha = \sqrt{2}/x$. This is shown as the thin solid line in the top panel, where the *continuous* matching of densities across $x_{\rm ew}$ is evident. The velocity field also joins continuously to the static $v \equiv 0$ at $x_{\rm ew}$. Table 3 lists $\alpha$, $v$, and the mass $m$ as functions of $x$ inside the head of the expansion wave. The initial radius $R$ of the cloud is fixed in real space (at least, until the expansion wave reaches it), and so over time moves steadily inwards in similarity space. The vertical lines in Fig. 3 are placed at $X = R/a_t t$ (eq. [3.6]), for the times $t/\bar{t}_{\rm ff}$ shown. As discussed above, $X = x_{\rm ew}$ after 1.80 free-fall times. Finally, the dashed lines in both panels of the Figure are just the free-fall profiles of equation (2.17). Clearly, they do not describe the flow until the gravitational attraction of the core exceeds the pressure-gradient force, at $x < 0.01$ or so.

A dimensional version of Fig. 3 is given in §4 below, but we now examine the dimensional core masses $M_0$ and accretion rates $\dot{M}_0 = 4\langle\dot{M}_0\rangle$ as functions of time in logotropes of various total

masses. These are obtained from equation (3.5):

$$M_0 = 5.41 \times 10^{-6}\ M_\odot \left(\frac{M_{\rm tot}}{M_\odot}\right) \left(\frac{\overline{t}_{\rm ff}}{4.8 \times 10^5\ {\rm yr}}\right)^{-4} \left(\frac{t}{10^5\ {\rm yr}}\right)^4$$
$$\dot{M}_0 = 2.16 \times 10^{-10}\ M_\odot\ {\rm yr}^{-1} \left(\frac{M_{\rm tot}}{M_\odot}\right) \left(\frac{\overline{t}_{\rm ff}}{4.8 \times 10^5\ {\rm yr}}\right)^{-4} \left(\frac{t}{10^5\ {\rm yr}}\right)^3 . \qquad (3.9)$$

It will be recalled (from Table 1 above) that $\overline{t}_{\rm ff} = 4.8 \times 10^5$ yr is appropriate for a solar-mass, $A = 0.2$ logotrope with temperature $T = 10$ K and surface pressure $P_s = 1.3 \times 10^5\ k\ {\rm cm}^{-3}$ K. The free-fall time of a logotrope with any other $M_{\rm tot}$, $P_s$, or $T$ can be computed as discussed in §2.1, so that equations (3.9) are quite generally applicable. The first of these relations is plotted in Fig. 4 for a number of different initial cloud masses. In a $C > \sqrt{2}$ collapse, our $M_0$ and $\dot{M}_0$ should each be multiplied by $(C/\sqrt{2})^{3/2}(m_0/6.67 \times 10^{-4})$, with $m_0$ taken, for example, from Table 2 above. What was already apparent from equation (3.5) is made more explicit here: a protostar in a collapsing logotrope gathers fully half of its mass $M_0$ over the last $1 - (0.5)^{1/4} \simeq 16\%$ of its accretion phase. By far the majority of a star's total formation time is spent waiting out a period of very slow and relatively unproductive infall in its parent cloud.

Also shown in Fig. 4 is the line $M_0 = 0.155\ M_\odot\ (t/10^5\ {\rm yr})(T/10\ {\rm K})^{3/2}$ for a singular isothermal sphere of *any* total mass. There are at least three points of interest in a comparison between this and the logotropic curves. (1) Any isothermal sphere has the *same* time-invariant accretion rate, while more massive logotropes eventually accrete much more rapidly than clouds of lower $M_{\rm tot}$. This is because a softer-than-isothermal EOS generally gives rise to larger nonthermal motions on larger scales, i.e., to higher $\sigma_{\rm ave}$ in higher-mass clouds (cf. §2.1). Roughly, then, since $\dot{M} \sim \sigma^3/G$, the mass originating from larger radii in bigger clouds will fall faster onto the core. (2) Generally speaking, low-mass stars take longer to accrete in a logotrope than in an isothermal sphere, while high-mass stars form on relatively shorter timescales. The extent of the discrepancy between the two models depends on the initial mass of the logotrope. Indeed, because of the effect noted in point (1), even the stellar mass for which the total accretion times coincide depends on $M_{\rm tot}$. (3) This being so, there is a much smaller spread in star-formation times in logotropes than in isothermal spheres. This is due to the weak mass dependence in the free-fall time of a logotrope (Table 1), and to the fact that $M_0 \propto (t/\overline{t}_{\rm ff})^4$. Specifically, stars of mass $0.3 M_\odot \le M_0 \le 30 M_\odot$ all tend to form within $1 - 3 \times 10^6$ yr, in logotropes of essentially any $M_{\rm tot}$. In an isothermal collapse, where $M_0 \propto t$, the accretion times would differ by a factor of 100.

It has to be recalled that these results are based on the assumption that the self-similar collapse solution continues to hold even after the expansion wave has been reflected from the boundary of a cloud. As discussed above, Fig. 4 may then represent upper limits to the true star-formation times in logotropes. On the other hand, this effect may not be very large; and in any case, it will be offset to some extent by the (outwards) radiation pressure from stars larger than a few $M_\odot$ (Jijina & Adams 1996). Our analysis should then be a reasonably accurate first-order approximation to a rather complicated situation.

These points could have some bearing on the formation of bound clusters, which requires that a large fraction ($\gtrsim$30%: Hills 1980; Lada, Margulis, & Dearborn 1984; Elmegreen & Clemens 1985) of the protocluster gas be converted to stars before the remainder is dispersed by supernovae or H II regions. In light of Fig. 4, and the short accretion times of high-mass stars, this would seem to demand that high-mass stars *start* collapsing *after* the low-mass stars do — a conclusion which also has ramifications for the form and origin of the stellar IMF.

Myers & Fuller (1992; also Myers & Fuller 1993; Caselli & Myers 1995) have introduced a "TNT" (thermal plus nonthermal) model of molecular clumps, which has an EOS that is explicitly isothermal at small radii, but becomes essentially polytropic (with $\gamma < 1$) at large $r$. They use this model to estimate approximate accretion times for stars of various masses. Although our logotropic model is preferable to the TNT construction (because the latter has density singularities at the centers of even pre-collapse, $t = -\infty$ clouds), the $M_0$ vs. $t$ relation of equation (3.9) and Fig. 4 may profitably be compared with that of Myers & Fuller. In particular, although our $t_{\rm end}$ for clouds of various masses tend to be somewhat longer than the TNT estimates — which bypass an exact treatment of the expansion wave, and which are almost isothermal for low-mass clumps anyway — they have roughly the same order of magnitude. More importantly, the rather narrow range in accretion times, and the fairly rapid formation of high-mass stars, are common to both sets of results; indeed, these are generic features of any softer-than-isothermal EOS.

## 4. Implications for Low-Mass Star Formation

Our analysis has concentrated on spherical infall in a logotrope, and ignored the effects of *mean* magnetic fields (to whatever extent disordered fields contribute to the turbulence in interstellar clouds, they are already accounted for by the EOS), rotation and circumstellar disks, and radiation pressure from the forming star. All of these have been studied analytically or numerically for accretion in isothermal clouds (e.g., Galli & Shu 1993a, b; Tereby et al. 1984; Boss & Black 1982; Jijina & Adams 1996, and references therein). In addition, some connection has to be made with the issues of fragmentation and binary formation (see, e.g., Myhill & Kaula 1992). Clearly, the present study can only be viewed as one step towards a full theory of non-isothermal collapse.

Nevertheless, some fairly robust conclusions can be drawn. In particular, although others have considered the effects of softer-than-isothermal, and even logotropic, equations of state on massive-star formation (e.g., Myers & Fuller 1992; Jijina & Adams 1996), the most important new point to be made here is that even low-mass ($\sim 1 M_\odot$) molecular clumps can be described by a logotropic EOS. Their collapse is therefore rather gentler than in the isothermal case, and their accretion rates must be much smaller at early times.

Figure 5 shows the time evolution, from $t = 5 \times 10^4$ to $t = 8.6 \times 10^5$ yr, of the density profile and velocity field in an expansion wave moving through an initially hydrostatic $A = 0.2$ logotrope

with a total mass of $1M_\odot$, a kinetic temperature $T = 10$ K (hence $\sigma_c = 1.88 \times 10^4$ cm s$^{-1}$), and a constant surface pressure $P_s = 1.3 \times 10^5\ k$ cm$^{-3}$ K. The velocity scale $a_t$ (eq. [2.10]) can be evaluated, at any time, given the surface pressure and the fact (cf. Table 1) that $P_c/P_s = 1.58$ in the non-singular cloud at $t = -\infty$; the dimensional $r$, $\rho$, and $u$ of Fig. 5 then follow immediately from the $x$, $\alpha$, and $v$ of Fig. 3. At the point $t = 0$ of core formation, the cloud is everywhere at rest and follows the singular density profile $\rho(r) = 1.3 \times 10^{-20}$ g cm$^{-3}$ $(r/R)^{-1}$. At later times, this profile still holds outside of the expansion wave; it is sketched as the broken line in the top panel of Fig. 5. For reference, we also have that the initial free-fall time of this cloud is $\bar{t}_{\rm ff} = 4.8 \times 10^5$ yr (Table 1); the initial ratio of central and mean densities is $\rho_c/\rho_{\rm ave} = 4.20$; and the initial radius is $R = 2.9 \times 10^{17}$ cm (eq. [3.4]; this is within a factor 2 of the radius of a solar-mass isothermal sphere under the same surface pressure). We have only plotted the densities and velocities for $t \leq 8.6 \times 10^5$ yr $= 1.80\ \bar{t}_{\rm ff}$, i.e., prior to the time $t_{\rm ew}$ when the head of the expansion wave meets the initial boundary of the cloud.

A cloud which is initially rotating at a constant rate $\Omega$ will depart from the spherical expansion-wave solution at small $r \lesssim R_C$, where $R_C$ is the *centrifugal radius* at which the circular speed $(GM_0/r)^{1/2}$ just equals the infall velocity $-u$. For an $M_{\rm tot} = 1M_\odot$ logotrope with the surface pressure and temperature we have assigned here, it is given by

$$R_C = \frac{\Omega^2 M_0}{2\pi A P_c} = 3.0 \times 10^{10}\ {\rm cm}\ \left(\frac{\Omega}{10^{-14}\ {\rm s}^{-1}}\right)^2 \left(\frac{t}{10^5\ {\rm yr}}\right)^4\ . \tag{4.1}$$

The first of these equalities comes from Jijina & Adams (1996; note the slightly different notation); the second, from our equation (3.9), along with $A = 0.2$ and the fact that $P_c = 1.58P_s$ for this specific example. Thus, a disk of 100 AU in extent will be built up within $\sim$1.5 $\times 10^6$ yr in our model, as compared to $\simeq$7.5 $\times 10^5$ yr for a singular isothermal sphere at $T = 10$ K. Scaling of this result for clouds with different total masses, surface pressures, and temperatures involves a change in the coefficient of $M_0$, as described after equation (3.9), and a change in $P_c/P_s$ from, e.g., Table 1. In any case, the magnitude of $R_C$ at a specified age $t$ gives some indication of the radial range in which the results of Fig. 5 are valid in an initially rotating cloud. Calculation of the analogous length scale for a magnetized sphere — the so-called magnetic radius of Galli & Shu (1993a, b) — will also be important, but is beyond the scope of this paper.

There are two main points to Fig. 5. The first is that the densities far behind the head of the expansion wave are well in excess of the initial hydrostatic values (see also Fig. 3 above), and are *increasing* with time. This is in stark contrast to an isothermal collapse, where $\rho(r)$ falls below its equilibrium value and decreases with time at small radii (cf. Fig. 3 of Shu 1977). The difference stems in part from the increasing $\dot{M}_0$ in our case, but more fundamentally from the fact that the initial $r^{-1}$ density profile of the logotrope is shallower than the final $r^{-3/2}$ which must obtain near the central core; there is relatively more mass in the outer regions of the static cloud than in the collapsing one, so a backlog of sorts develops at small radii. The opposite is true of a singular isothermal sphere, which begins with a static $r^{-2}$ density profile. More quantitatively, the scaling $\alpha \propto x^{-3/2}$ implies $\rho(r,t) \propto r^{-3/2}t$ for the logotrope, but $\rho(r,t) \propto r^{-3/2}t^{-1/2}$ for an isothermal

EOS.

This situation calls to mind observations of the far-infrared emission of the NGC 2071 region in Orion B (Butner et al. 1990). Radiative-transport models are consistent with a central star of around $5M_{\odot}$ there, and a $\rho \propto r^{-3/2}$ density profile at radii $r \geq 2000$ AU. However, the value of the density at 2000 AU given by Butner et al.'s radiative transport analysis (and also suggested by independent molecular data) is at least one full order of magnitude *larger* than that expected for an isothermal expansion-wave collapse. One explanation for this is that 2000 AU is deep inside the expansion wave for an isothermal collapse age of $\simeq 5 \times 10^5$ yr (which follows from an assumed $T = 35$ K and $M_0 = 5M_{\odot}$), such that significant depletion would have occurred there. There is no such depletion, but rather an enhancement, in our logotropic model, and these data could therefore provide an important test of it. However, a proper analysis of NGC 2071 would require a self-consistent treatment of radiation pressure and rotation, as well as a reliable feel for the initial total mass involved, and is too detailed to be undertaken here.

The second point of Fig. 5 is that, naturally, the infall velocity at any given radius also grows over time, *but* at a rate which is quite different from that in an isothermal sphere. In particular, since $u \propto (M_0/r)^{1/2}$ at small radii, we have that $u \propto r^{-1/2}t^2$ in a logotrope, while $u \propto r^{-1/2}t^{1/2}$ in the isothermal case. At any fixed $r$, the velocities in the two models will agree at some $t$; the logotropic $u$ must then be smaller than the isothermal one at earlier times, and larger later on. With $M_{\rm tot} = 1M_{\odot}$ specifically, a comparison of Fig. 5 and Shu's (1977) Fig. 3 shows that we are firmly in the former, lower-velocity regime at all radii and throughout the entire duration $t \leq t_{\rm ew}$.

For example, let us focus on the scale $r = 10^{16}$ cm $\simeq 0.003$ pc. Our model gives infall velocities there (and at larger radii) which are *less than the thermal linewidth*, $\sigma_c \simeq 0.2$ km s$^{-1}$, for all $t \leq 8.6 \times 10^5$ yr. By contrast, a solar-mass, singular isothermal sphere attains $-u \simeq \sigma_c$ at the same radius by $t = 6 \times 10^4$ yr. This is one example of how the systematic velocity field at observable radii in a logotrope of *any* mass will be effectively swamped by random velocities for a significant fraction of the duration of its collapse; even a molecular clump which is well into the accretion phase can appear to be in virial equilibrium. Because the accretion rate increases with time, at any instant the majority of clumps will be in a fairly inconspicuous evolutionary state. This could explain the apparent paucity of obviously collapsing regions of the ISM. Similarly, for those clouds which do show observable signatures of collapse, the adoption of a logotropic EOS leads to larger inferred dynamical ages than an isothermal model would suggest.

Currently the best direct, kinematic evidence for collapse is in the isolated Bok globule B335, where molecular line profiles appear consistent with infall velocities $-u \sim 1.2$ km s$^{-1}$ at radii $r \sim 5 \times 10^{15}$ cm (Zhou et al. 1993). Given that $-u = (2GM_0/r)^{1/2}$ deep inside any expansion wave (which radial scaling is also consistent with the B335 data), this implies the existence of a central protostar (or star plus disk) with mass $M_0 \simeq 0.25M_{\odot}$. As well, 1.3-mm continuum measurements of dust emission indicate a circumstellar envelope of about $0.8M_{\odot}$ (Bontemps et al. 1996). The physical parameters which we have specified in deriving Fig. 5 therefore seem particularly

suited to a discussion of B335.[2] In particular, *model-independent* considerations suggest that $M_0/M_{\rm tot} \sim 0.25$ in this object. If it is undergoing a logotropic collapse, it must then be older than $t_{\rm ew} = 8.6 \times 10^5$ yr, because our similarity solution gives a much smaller $M_0/M_{\rm tot} = 0.03$ at that time. (In addition, Fig. 5 shows that $-u$ is rather less than the observed value at $r = 5 \times 10^{15}$ cm for all $t \le t_{\rm ew}$.) That is to say, *the expansion wave should already have been reflected from the boundary of B335.*

If B335 is much older than $t_{\rm ew}$, then it will no longer follow its original $r^{-1}$ density profile; the entire cloud should be taken up in the collapse and the free-fall $\rho \propto r^{-3/2}$ should hold essentially throughout. In fact, this is consistent with the study of Zhou et al. (1990), who conclude that the densities in the inner regions of the globule are best described by an $r^{-1.5}$ power law. (As a test of the isothermal collapse theory specifically, they go on to argue that at large radii the densities are consistent with $\rho \propto r^{-2}$. However, there is no *direct* evidence for this, or for any other power law but $-1.5$; the data are "insufficient to determine independently the parameters of a density distribution with two power-law regimes" [Zhou et al. 1990].)

Just how old is B335? Equation (3.9), given $M_0 = 0.25 M_\odot$, predicts a collapse age of $t = 1.5 \times 10^6$ yr (if our fiducial surface pressure is correct here), and hence a time-averaged accretion rate of $\langle \dot{M}_0 \rangle = M_0/t = 1.7 \times 10^{-7} M_\odot$ yr$^{-1}$. These numbers are, moreover, quite robust again any uncertainties in the initial total mass: even for an unrealistically extreme $M_{\rm tot} = 10 M_\odot$ (in which case $M_0/M_{\rm tot} \sim 0.03$ and the expansion wave would have just reached the edge of the cloud), we find $t \simeq 1.2 \times 10^6$ yr. By contrast, Zhou et al. (1993) discuss their data in terms of the isothermal expansion wave model and estimate $t = 1.5 \times 10^5$ yr, $\dot{M}_0 = 2.8 \times 10^{-6} M_\odot$ yr$^{-1}$, and $M_0 = 0.4 M_\odot$. It seems inevitable that our model requires an age for B335 which is nearly an order of magnitude older, with a time-averaged accretion rate that much smaller, than previously thought.

B335 is an example of the low-mass "Class 0" sources recently identified by André et al. (1993) and André & Montmerle (1994). These typically have (cold) single-blackbody spectral energy distributions, but are invisible at short wavelengths $\lambda \lesssim 10$ $\mu$m. This is attributed to veiling by a circumstellar envelope whose mass exceeds that of the central protostar — a conclusion which is supported by direct, mm-continuum measurements of the envelope masses — and therefore implies that these objects are in the earliest stages of collapse yet to be observed. Indeed, the theory of isothermal accretion applied to the Class 0 sources generally implies ages of a few $10^4$ yr (e.g., Barsony 1994; Pudritz et al. 1996). Although B335 might then be somewhat older than average even in the context of isothermal models, it seems likely that the relative age increase

[2]In fact, Zhou et al. (1990) favor a kinetic temperature of 13 K for B335. A $T = 13$ K logotrope with no mean magnetic field has a critical mass of $155 M_\odot$ and a free-fall time of $6.6 \times 10^5$ yr, by equations (2.2) and (2.3). Thus, B335 has $M_{\rm tot}/M_{\rm crit} \simeq 0.0064$, and hence a truncation radius $R/r_0 \simeq 1$ from Table 1. This in turn implies $\overline{t}_{\rm ff}/\overline{t}_{\rm ff,crit} \simeq 0.74$, or $\overline{t}_{\rm ff} = 4.9 \times 10^5$ yr. Our timescale estimates, which strictly apply to a $T = 10$ K solar-mass logotrope with $\overline{t}_{\rm ff} = 4.8 \times 10^5$ yr, are then relevant to B335 as well.

we deduce for it should also be applied to other Class 0 sources. Note, though, that most of this age increase is required to accomodate an early period of very gentle infall, with small central source masses and low accretion luminosities. *Most* of a $1M_{\odot}$ star is accreted over a period of only $\sim 2 - 3 \times 10^5$ yr in a logotrope. This is much smaller than the total collapse time (cf. Fig. 4) and is still consistent, for example, with empirical estimates of the formation time of visible T Tauri stars in the Taurus-Auriga complex (Myers & Benson 1983; Myers et al. 1987).

Finally, if our low mean accretion rate in B335 is typical, then it should have some bearing on the "luminosity problem" of young stellar objects in Taurus-Auriga. Very briefly, the bolometric luminosities of Class I sources there (which are embedded in less massive circumstellar envelopes than Class 0's, and hence appear to be in later stages of collapse; André & Montmerle 1994) are generally about an order of magnitude smaller than expected from number-count arguments (Kenyon et al. 1990; Kenyon et al. 1994) and fits to individual spectral energy distributions (Kenyon, Calvet, & Hartmann 1993; see also Adams, Lada, & Shu 1987). A similarly low luminosity has also been noted for the prototypical Class 0 source VLA 1623 (Pudritz et al. 1996). The problem derives, in large part, from the isothermal assumption of a time-independent accretion rate $\dot{M}_0$, and Kenyon et al. note that it could be alleviated if stars accumulate most of their mass on timescales which are short compared to the total duration of their embedded phase. We have seen that such a situation arises naturally in the collapse of a logotrope. A revision of the assumed EOS in molecular clouds may therefore play an important part in the eventual resolution of this issue.

## 5. Summary

McLaughlin & Pudritz (1996) have shown that a logotropic equation of state, $P/P_c = 1 + A\ \ln(\rho/\rho_c)$ and $A = 0.2$, provides the most self-consistent description of the internal, equilibrium structure of both low- and high-mass dense clumps within GMCs, and of the global properties (Larson's laws) of the giant cloud complexes themselves. We have now used this model to investigate the collapse of interstellar clouds. There are a number of consequences for issues of not only high-mass, but also low-mass, star formation.

We have derived similarity solutions for the collapse of a gaseous logotrope. These solutions are analogous to those of Shu (1977) for the collapse of singular isothermal spheres; in particular, an expansion-wave solution — the inside-out collapse of a cloud which is initially in virial equilibrium — is identified as the one of most physical interest. The predicted density profile is $\rho \propto r^{-1}$ for gas which has not yet been reached by the expansion wave, and $\rho \propto r^{-3/2}$ far behind the collapse front, where infall velocities approach their free-fall values $-u = (2GM_0/r)^{1/2}$. These latter scalings are model-independent, as they follow directly from the presence of a central point mass (protostar) $M_0$. However, the core accretion rate in a logotrope increases with time (as $\dot{M}_0 \propto t^3$, so that $M_0 \propto t^4$), while it is constant for an isothermal sphere.

This implies that $\dot{M}_0$ in a logotrope will be smaller than the isothermal value at early times, and larger at late times. Low-mass stars therefore take longer to form, while high-mass stars are built up much more rapidly. With $\bar{t}_{\rm ff}$ the mean free-fall time of a logotrope (typically of order $5 \times 10^5$ yr), our similarity solutions are strictly valid for $t < 1.8\bar{t}_{\rm ff}$. At that point the expansion wave reaches the edge of a cloud — with only 3% of the total initial mass having been accreted onto the core — and hydrodynamical simulations will likely be required to exactly describe the later stages of evolution in which most of the final mass of a star is accreted. Nevertheless, a simple extrapolation of our present results suggests that if a cloud of any mass were to completely collapse to a single star, it would do so by $t = 4.3\ \bar{t}_{\rm ff}$. A weak dependence of $\bar{t}_{\rm ff}$ on mass in logotropes, together with the result $M_0 \propto t^4$, guarantees that the accretion times of stars of widely disparate masses differ only slightly: stars of anywhere from 0.3 to $30 M_\odot$ are all expected to form within $\sim 1 - 3 \times 10^6$ yr. This conclusion, which is similar to that reached in other studies of non-isothermal collapse, has important implications for cluster formation and the stellar IMF.

Another clear difference between the logotropic and isothermal models lies in the evolution of the density at small radii in a cloud: $\rho$ ultimately increases with time at any given radius in our model, but would decrease in a singular isothermal sphere. Infall velocities $u$, on the other hand, grow with time in any collapse model, but the *rates* at which they do so are quite dependent on the assumed equation of state. Early on in its collapse, the logotrope can have much smaller $u$ than an isothermal sphere. It therefore takes longer for observable systematic velocities to develop at observable radii within a cloud, and collapse will initially be harder to detect directly. This implies that (1) early on in its accretion phase, a logotrope will effectively appear to still be in virial equilibrium, such that the number of molecular clumps which are in fact undergoing collapse could be much larger than previously suspected; and (2) current estimates for the ages of (low-mass) young stellar objects, which are based on isothermal collapse models, should be subject to a significant upwards revision. In the Bok globule B335 specifically, we find an age which is certainly greater than $8.6 \times 10^5$ yr, and probably $\sim 1.5 \times 10^6$ yr, older by perhaps an order of magnitude than suggested by the isothermal expansion-wave theory. This result could have wider implications for the ages of Class 0 protostars (of which B335 is one) in general.

This work was supported in part by the Natural Sciences and Engineering Research Council of Canada.

## A. COLLAPSING POLYTROPES

### A.1. Similarity Solutions

In many ways, the isothermal sphere and the logotrope are profitably viewed as opposite extremes of the family of *negative-index polytropes*, which have $P \propto \rho^\gamma$ with $0 < \gamma \leq 1$. Although incomplete as models of real interstellar clouds, these have been considered, for example, by

Maloney (1988), McKee & Zweibel (1995), and MP96. The case $\gamma = 1$ gives an isothermal equation of state, while most features of the logotrope are recovered by formally setting $\gamma = 0$ in what follows. The "negative-index" label refers to standard polytropic notation, which has $\gamma = 1 + 1/N$. An isothermal EOS then corresponds to $N \rightarrow -\infty$; the logotrope, to $N \rightarrow -1$.

To derive similarity solutions for collapsing polytropes, we write the EOS as

$$P = K\rho^{\gamma} \ . \tag{A1}$$

The similarity variable $x$, the dimensionless density $\alpha$, the velocity $v$, and the mass $m$ are all defined as in equations (2.8) and (2.9) above; and since $dP/d\rho = K\gamma\rho^{\gamma-1}$, the appropriate velocity scale is just

$$a_t = \left[K\gamma(4\pi G t^2)^{1-\gamma}\right]^{1/2} \ . \tag{A2}$$

As discussed in §2.1, we are concerned with the evolution of a cloud only *after* the time $t = 0$ when a core has formed at its center. The density structure is then singular throughout, and $K$ is a constant in space and time, with the value $\sigma_c^2\rho_c^{\gamma-1}$ it had in the initial ($t = -\infty$) cloud.

If we write

$$\beta \equiv (2-\gamma)x - v \ , \tag{A3}$$

then equations (2.5) – (2.7) give the following:

$$\left[\beta^2 - \alpha^{\gamma-1}\right]\frac{d\,\ln\alpha}{dx} = \left[\frac{\alpha}{4-3\gamma} - \frac{2}{x}\beta\right]\beta + (1-\gamma)\left[2\beta + v\right] \tag{A4}$$

$$\left[\beta^2 - \alpha^{\gamma-1}\right]\frac{dv}{dx} = \left[\frac{\alpha}{4-3\gamma}\beta - \frac{2\alpha^{\gamma-1}}{x}\right]\beta + (1-\gamma)\left[2\alpha^{\gamma-1} + v\beta\right] \tag{A5}$$

$$m = \frac{\alpha x^2}{4-3\gamma}\beta \ . \tag{A6}$$

Setting $\gamma = 1$ in expressions (A2) onwards recovers the results of Shu (1977) for the isothermal sphere; if instead $\gamma = 0$ (but $K\gamma$ is replaced by $AP_c$), then the equations of our §2.2 are obtained. No constraint has yet been imposed on the value of $\gamma$, and in particular it could well be $> 1$ at this point. In this regime, treatment of the case $\gamma = 4/3$ evidently requires some care. We do not discuss this point further, but note that it relates to the instability of positive-index polytropes with $1 < \gamma < 4/3$ (e.g., Chandrasekhar 1967). Goldreich & Weber (1980) have studied the *homologous* collapse of a $\gamma = 4/3$ polytrope, in connection with the evolution of degenerate iron cores in supernovae. More generally, Suto & Silk (1988) solve equations for the self-similar collapse of polytropes with arbitrary indices $\gamma$. The physical requirement $K =$ constant identifies our equations (A4) and (A5) with equations (15) of Suto & Silk, in their "$n = 2 - \gamma$" case.

Still without restricting the value of $\gamma$, equations (A4) – (A6) admit two analytic solutions. One of these is the same uniform-density case given by equation (2.14); the other is the static solution,

$$\alpha = C_{\rm HSE}\ x^{-2/(2-\gamma)} \qquad v \equiv 0 \qquad m = \frac{2-\gamma}{4-3\gamma}\ C_{\rm HSE}\ x^{(4-3\gamma)/(2-\gamma)} \ , \tag{A7}$$

where the density normalization is

$$C_{\rm HSE} = \left[\frac{2(4-3\gamma)}{(2-\gamma)^2}\right]^{1/(2-\gamma)} \quad . \tag{A8}$$

The singular density profile thus obtained is an exact solution of the equation of hydrostatic equilibrium for a self-gravitating polytrope of any (negative) index (cf. MP96). Again, if $\gamma = 0$ here, the logotropic result (2.15) obtains, while if $\gamma = 1$ we have $\alpha = 2/x^2$ and $m = 2x$, in agreement with Shu (1977) for the singular isothermal sphere.

In the context of interstellar clouds, we are interested only in the range $0 < \gamma \le 1$ — and particularly the $\gamma = 0$ limit of the logotrope — since the velocity dispersion $P/\rho$ then increases with radius. For such $\gamma$, equations (A4) – (A6) in the limit $x \to 0$ (late times or small radii) and $|v| \gg x$ give

$$\alpha \to (4-3\gamma)\left(\frac{m_0}{2x^3}\right)^{1/2} \qquad v \to -\left(\frac{2m_0}{x}\right)^{1/2} \qquad m \to m_0 \ , \tag{A9}$$

which are minus solutions. In the opposite limit $x \to \infty$ (early times or large radii) and $|v| \ll x$, we have instead

$$\alpha \to Cx^{-2/(2-\gamma)} \qquad v \to -\frac{2-\gamma}{4-3\gamma}\, C\left[1-\left(\frac{C_{\rm HSE}}{C}\right)^{2-\gamma}\right] x^{-\gamma/(2-\gamma)} \qquad m \to \frac{2-\gamma}{4-3\gamma}\, Cx^{(4-3\gamma)/(2-\gamma)} \ . \tag{A10}$$

The density normalization $C$ is essentially a free parameter, but it must exceed the hydrostatic equilibrium value $C_{\rm HSE}$ (eq. [A8]) for inflow ($v < 0$). As usual, then, this family of solutions represents the collapse of non-equilibrium spheres which are everywhere denser (by a factor $C/C_{\rm HSE}$) than a virialized one with the same volume. There is also a one-to-one relationship between $C$ and $m_0$ for a complete solution which extends from $x = \infty$ (the moment of core formation) to $x = 0$ (the end of accretion), and the limit $C \to C_{\rm HSE}^{+}$ corresponds to the expansion-wave solution. (Note that these asymptotic solutions differ from those cited by Larson [1969], which hold for plus solutions where $|v|$ increases at large $x$ but is still $\ll x$. A sufficient, though not necessary, condition for the existence of such solutions is $\gamma > 1/3$.)

### A.2. Accretion Rates

The reduced core mass $m_0$ translates, by equations (A2) and (2.9), to a dimensional

$$M_0 = \gamma^{3/2}\left(\frac{3\pi^2}{8}\frac{\rho_c}{\rho_{\rm ave}}\right)^{3(1-\gamma)/2} \frac{t^{4-3\gamma}}{\bar{t}_{\rm ff}^{\,3-3\gamma}}\ \frac{m_0\sigma_c^3}{G} \ , \tag{A11}$$

where $\bar{t}_{\rm ff}$ is the free-fall time evaluated at the initial mean density $\rho_{\rm ave}$, and where we have used the fact that $K = \sigma_c^2\rho_c^{1-\gamma}$. By construction, the linewidth $\sigma_c$ at the center of a cloud is taken to be

purely thermal — $\sigma_c^2 = kT/\mu m_H$ — and the EOS automatically accounts for nonthermal motions elsewhere. In any case, the mass accretion rate is therefore

$$\dot{M}_0 = (4-3\gamma)\gamma^{3/2}\left(\frac{3\pi^2}{8}\frac{\rho_c}{\rho_{\rm ave}}\right)^{3(1-\gamma)/2}\left(\frac{t}{\overline{t}_{\rm ff}}\right)^{3(1-\gamma)}\frac{m_0\sigma_c^3}{G} = (4-3\gamma)\langle\dot{M}_0\rangle\ , \tag{A12}$$

and only the singular isothermal sphere has an accretion rate $\dot{M}_0 = \langle\dot{M}_0\rangle = m_0\sigma_c^3/G$ that is constant in time. Formally, the results of §3 above are recovered by substituting $A^{3/2}$ for $\gamma^{3/2}$ and setting $\gamma = 0$ elsewhere in these expressions.

Now, by manipulating the results given in Appendix C of MP96, the total mass and radius of a *singular* pressure-truncated polytrope can be written as

$$M_{\rm tot} = \frac{8}{\pi}\left(\frac{3\gamma}{4-3\gamma}\right)^{3/2}\left(\frac{4-3\gamma}{6-3\gamma}\right)^{3\gamma/2}\left(\frac{C}{C_{\rm HSE}}\right)^{3/2}\left(\frac{\rho_c}{\rho_{\rm ave}}\right)^{3(1-\gamma)/2}\overline{t}_{\rm ff}\frac{\sigma_c^3}{G} \tag{A13}$$

and

$$R = \frac{4}{\pi}\left(\frac{3\gamma}{4-3\gamma}\right)^{1/2}\left(\frac{4-3\gamma}{6-3\gamma}\right)^{\gamma/2}\left(\frac{C}{C_{\rm HSE}}\right)^{1/2}\left(\frac{\rho_c}{\rho_{\rm ave}}\right)^{(1-\gamma)/2}\overline{t}_{\rm ff}\sigma_c\ , \tag{A14}$$

which should be compared to equations (3.3), (3.4) in the logotropic limit $\gamma = 0$. The factor $C/C_{\rm HSE}$ here is required for consideration of the collapse (A10) of a sphere which is everywhere denser than a virial-equilibrium configuration with the same radius $R$ and temperature $\sigma_c$. Where the expansion wave is concerned, of course, the initial cloud is taken to be exactly virialized, and $C = C_{\rm HSE}$.

Given these results, the central point mass builds up as

$$\frac{M_0}{M_{\rm tot}} = \frac{\pi}{8}\left(\frac{\pi^2}{8}\frac{4-3\gamma}{2-\gamma}\right)^{3(1-\gamma)/2}\left(\frac{1}{2-\gamma}\frac{C}{C_{\rm HSE}}\right)^{-3/2}\left(\frac{t}{\overline{t}_{\rm ff}}\right)^{4-3\gamma} m_0\ , \tag{A15}$$

and the boundary $X = R/a_t t$ is given by

$$X = \frac{4}{\pi}\left(\frac{8}{\pi^2}\frac{2-\gamma}{4-3\gamma}\right)^{(1-\gamma)/2}\left(\frac{1}{2-\gamma}\frac{C}{C_{\rm HSE}}\right)^{1/2}\left(\frac{t}{\overline{t}_{\rm ff}}\right)^{\gamma-2}\ . \tag{A16}$$

If our similarity solution is taken to hold at all times, then equation (A15) gives the time to accrete an entire cloud onto the core ($M_0/M_{\rm tot} = 1$). For the expansion wave, with $C = C_{\rm HSE}$, this ranges between $t_{\rm end} \simeq 2.61\ \overline{t}_{\rm ff}$ for $\gamma = 1$, and $t_{\rm end} \simeq 4.32\ \overline{t}_{\rm ff}$ for $\gamma = 0$. (The relation between $\gamma$ and $m_0$ is given by Table 4 in Appendix B.) Strictly speaking, however, boundary effects are important at late times in finite spheres; in particular, the expansion wave will reach the edge of a cloud when $X = x_{\rm ew}$ (eqs. [B3], [B4]), i.e., at

$$t_{\rm ew} = \frac{4\sqrt{2-\gamma}}{\pi}\ \overline{t}_{\rm ff} < t_{\rm end}\ . \tag{A17}$$

## B. CRITICAL POINTS

Collapse flows in polytropes with $\gamma \leq 1$ (where again $\gamma$ is set to 0 for the logotrope) may involve passage through a critical point, $x_* \geq 0$, where the velocity $v_* \leq 0$ and density $\alpha_*$ satisfy

$$(2-\gamma)x_* - v_* = \alpha_*^{(\gamma-1)/2} \ . \tag{B1}$$

Equations (A4) and (A5) then demand that

$$\frac{\alpha_*^{(\gamma+1)/2}}{4-3\gamma} + (1-\gamma)\alpha_*^{(\gamma-1)/2} - \frac{2}{x_*}\alpha_*^{\gamma-1} + (1-\gamma)(2-\gamma)x_* = 0 \tag{B2}$$

in order for $(d\alpha/dx)_{x_*}$ and $(dv/dx)_{x_*}$ to be finite.

The critical point $x_{\rm ew}$ for which $v_* = 0$ has, by (B1),

$$x_{\rm ew} = \frac{\alpha_{\rm ew}^{(\gamma-1)/2}}{2-\gamma} \ , \tag{B3}$$

so that (B2) gives

$$\alpha_{\rm ew} = 2(4-3\gamma) = \left[\frac{2(4-3\gamma)}{(2-\gamma)^2}\right]^{1/(2-\gamma)} x_{\rm ew}^{-2/(2-\gamma)} \ , \tag{B4}$$

which agrees with the static solution (eqs. [A7], [A8]) of the fluid equations at $x_{\rm ew}$. The collapse solution which begins with $v \to -\infty$ at $x = 0$, and goes on to pass through $x_{\rm ew}$ with $v = 0$, may therefore be continued to larger $x$ by attaching the static solution. This composite flow is just the expansion wave.

We now confine our attention to critical points $x_* \leq x_{\rm ew}$, so that $v_* \leq 0$ and $\alpha_* \geq \alpha_{\rm ew}$. In general, given $x_*$, it is a simple matter to find $\alpha_*$ and $v_*$ from equations (B2) and (B1). We then set

$$\alpha(x) = \alpha_* + a_1(x-x_*) + \mathcal{O}[(x-x_*)^2] \qquad \text{and} \qquad v(x) = v_* + b_1(x-x_*) + \mathcal{O}[(x-x_*)^2]$$

in some neighborhood of $x_*$. Substitution of this first-order expansion in equations (A4) and (A5) leads to a pair of coupled quadratic equations for the slopes $a_1$ and $b_1$. Under the constraint (B2), these yield a single cubic equation for $a_1$, and thus three eigensolutions for the flow through a critical point. The first of these satisfies the simple relation

$$b_1 = (2-\gamma) + \frac{1-\gamma}{2} a_1 \alpha_*^{(\gamma-3)/2} \ , \tag{B5}$$

which serves only to move the flow along the locus (B1) of critical points. Such a propagation of singularities is so contrived as to be unphysical, and we therefore discard this solution. This leaves us with

$$\begin{aligned} a_1 &= -\left[\frac{k_1 \pm \sqrt{k_1^2 - 4(1+\gamma)k_2}}{2(1+\gamma)}\right] \alpha_*^{(3-\gamma)/2} \\ b_1 &= -2(1-\gamma) + \frac{2}{x_*}\alpha_*^{(\gamma-1)/2} + a_1\alpha_*^{(\gamma-3)/2} \ , \end{aligned} \tag{B6}$$

where

$$k_1 \equiv -(9-7\gamma) + \frac{8}{x_*}\alpha_*^{(\gamma-1)/2}$$
$$k_2 \equiv \alpha_* + 2(1-\gamma)(5-3\gamma) - \frac{4(4-3\gamma)}{x_*}\alpha_*^{(\gamma-1)/2} + \frac{6}{x_*^2}\alpha_*^{\gamma-1} \ . \tag{B7}$$

For $x_* \leq x_{\rm ew}$ and $0 \leq \gamma \leq 1$, $a_1$ is always real and negative. If the '$-$' sign is taken to solve for it in equation (B6), we find $b_1 \geq 0$, and such solutions have $v$ more negative at smaller $x$. These therefore correspond to the minus solutions of Shu (1977), or the type 2 solutions of Hunter (1977) and Whitworth & Summers (1985). In the isothermal limit of $\gamma = 1$, the result is $a_1 = -2/x_*^2$ and $b_1 = 1/x_*$. If instead the '+' sign is taken in equation (B6), then $b_1 \leq 0$ and we recover the plus (or type 1) solutions; in the isothermal case, $a_1 = 2/x_* - 6/x_*^2$ and $b_1 = 1 - 1/x_*$. The plus solutions for this or any other $\gamma$ have $|v|$ growing for $x > x_*$, and vanishing at some nonzero $x < x_*$. In addition, they are underdense at large $x$, relative to the singular hydrostatic profile, and may therefore be of interest as (time-reversed) wind solutions.

The slopes $a_1$ and $b_1$ at $x_{\rm ew}$ can be found analytically, given any $\gamma$, for both the minus and the plus solutions which flow through that point; again, the minus solution at $x_{\rm ew}$ is the expansion wave. Using equations (B3) and (B4) in (B6) and (B7), we have the following:

- $3/5 < \gamma \leq 1$, *minus solution*:

$$a_1 = \frac{3\gamma-5}{1+\gamma}\alpha_{\rm ew}^{(3-\gamma)/2} < 0 \qquad \text{and} \qquad b_1 = \frac{5\gamma-3}{1+\gamma} > 0 \ . \tag{B8}$$

  Although $\alpha_{\rm ew}$ and $v_{\rm ew}$ match the density and velocity of the corresponding static solution at $x_{\rm ew}$, the derivatives do *not* agree there (in particular, $dv/dx \equiv 0$ for the static outer cloud). The density profile and velocity field of an expansion wave in this range of $\gamma$ — which includes the isothermal sphere — are therefore discontinuous at $x_{\rm ew}$.

- $0 \leq \gamma \leq 3/5$, *minus solution*:

$$a_1 = -2\alpha_{\rm ew}^{(3-\gamma)/2} < 0 \qquad \text{and} \qquad b_1 = 0 \ . \tag{B9}$$

  Now these (left) derivatives do match the (right) derivatives of the static solution at the head $x_{\rm ew}$ of the expansion wave (see eq. [A7]), and the full flow is everywhere continuous. The logotrope corresponds to $\gamma = 0$, and therefore shows this behavior.

The plus solutions at $x_{\rm ew}$ for $\gamma > 3/5$ have the same $a_1$ and $b_1$ as the minus solutions for $\gamma \leq 3/5$; and the plus solutions at $x_{\rm ew}$ for $\gamma \leq 3/5$ have the same derivatives as the minus solutions for $\gamma > 3/5$.

Equations (B8) and (B9) also show that, for $\gamma < 1$, the velocity slope $b_1$ of the expansion wave at $x_{\rm ew}$ is always shallower than the gradient $dv_*/dx_*$ of the locus (B1) of critical points there,

and the infall velocity of the material just inside the head of the wave is less than the critical value. However, $|v|$ increases without bound towards $x = 0$ for a minus solution, so any gas EOS which is softer than isothermal (including logotropic; §2.3) leads to an expansion-wave flow that eventually crosses a second critical point $x_* < x_{\rm ew}$. Since the expansion wave also stands as the limit of out-of-equilibrium collapse solutions ($C > C_{\rm HSE}$; Appendix A), some of these must also pass through two critical points. By contrast, in the isothermal case the expansion wave is just tangent to the locus of critical points at $x_{\rm ew} = 1$, and all $C > 2$ infall solutions avoid it altogether.

Finally, it is clear that the head $x_{\rm ew}$ of the expansion wave; its second, inner critical point $x_*$; and the core mass/central accretion rate $m_0$ are all uniquely defined by the specification of the polytropic index $\gamma$. These connections are shown in Table 4. Also given there is the total mass $m_{\rm ew}$ interior to $x_{\rm ew}$ (from eq. [A7]). The ratio $m_0/m_{\rm ew}$ is the fraction of infalling material which is already taken up in the central core itself.

Table 1. Properties of Pressure-Truncated $A = 0.2$ Logotropes.

| $R/r_0$ | $\rho_c/\rho_s$ | $P_c/P_s$ | $\rho_{\rm ave}/\rho_c$ | $\sigma^2_{\rm ave}/\sigma^2_c$ | $M_{\rm tot}/M_\odot$ [a] | $\bar{t}_{\rm ff}/10^5$ yr [a] |
|---|---|---|---|---|---|---|
| 0.93 | 4.28 | 1.41 | 0.335 | 2.3 | 0.5 | 4.2 |
| 1.34 | 6.22 | 1.58 | 0.238 | 2.9 | 1 | 4.8 |
| 2.45 | 11.54 | 1.96 | 0.130 | 4.4 | 3 | 5.9 |
| 4.85 | 23.01 | 2.68 | 0.0655 | 6.7 | 10 | 7.1 |
| 9.40 | 44.63 | 4.16 | 0.0337 | 9.1 | 30 | 7.9 |
| 13.18 | 62.56 | 5.79 | 0.0240 | 10.0 | 50 | 7.9 |
| 17.02 | 80.77 | 8.22 | 0.0186 | 10.1 | 70 | 7.6 |
| 19.26 | 91.39 | 10.32 | 0.0164 | 10.0 | 80 | 7.2 |
| 21.26 | 100.88 | 12.95 | 0.0149 | 9.3 | 87 | 6.7 |
| 24.37[b] | 115.58 | 20.00 | 0.0130 | 9.0 | 92 | 5.8 |

[a]Calculated assuming no mean magnetic field; surface pressure $P_s = 1.3 \times 10^5\ k\ {\rm cm}^{-3}$ K; and kinetic temperature $T = 10$ K.

[b]Truncation radius of a critically stable cloud, $M_{\rm tot} = M_{\rm crit}$.

Table 2. Core Mass vs. Density Normalization.

| $C$ | $m_0$ |
|---|---|
| $\sqrt{2}+\epsilon$ | 0.000667 |
| 1.42 | 0.00173 |
| 1.4245 | 0.00248 |
| 1.43 | 0.00339 |
| 1.44 | 0.00507 |
| 1.46 | 0.00869 |
| 1.48 | 0.0127 |
| 1.50 | 0.0170 |
| 1.53 | 0.0243 |
| 1.56 | 0.0323 |
| 1.60 | 0.0444 |
| 1.70 | 0.0808 |
| 1.90 | 0.182 |
| 2.20 | 0.409 |
| 2.60 | 0.871 |

Table 3. Logotrope Expansion Wave.

| $x$ | $\alpha$ | $-v$ | $m$ | $x$ | $\alpha$ | $-v$ | $m$ |
|---|---|---|---|---|---|---|---|
| 0 | $\infty$ | $\infty$ | 0.000667 | 0.085 | 16.0 | 0.0102 | 0.00522 |
| 0.001 | 2395 | 1.115 | 0.000668 | 0.090 | 15.2 | 0.00846 | 0.00582 |
| 0.002 | 879 | 0.760 | 0.000671 | 0.095 | 14.5 | 0.00697 | 0.00646 |
| 0.003 | 497 | 0.599 | 0.000675 | 0.100 | 13.9 | 0.00570 | 0.00713 |
| 0.004 | 335 | 0.500 | 0.000680 | 0.105 | 13.3 | 0.00463 | 0.00784 |
| 0.005 | 249 | 0.431 | 0.000686 | 0.110 | 12.7 | 0.00371 | 0.00859 |
| 0.010 | 106 | 0.254 | 0.000728 | 0.115 | 12.2 | 0.00294 | 0.00938 |
| 0.015 | 68.9 | 0.175 | 0.000793 | 0.120 | 11.7 | 0.00230 | 0.0102 |
| 0.020 | 52.4 | 0.129 | 0.000884 | 0.125 | 11.2 | 0.00176 | 0.0111 |
| 0.025 | 43.2 | 0.0988 | 0.00100 | 0.130 | 10.8 | 0.00132 | 0.0120 |
| 0.030 | 37.2 | 0.0781 | 0.00115 | 0.135 | 10.4 | 0.000965 | 0.0129 |
| 0.035 | 32.9 | 0.0630 | 0.00134 | 0.140 | 10.1 | 0.000680 | 0.0139 |
| 0.040 | 29.6 | 0.0515 | 0.00156 | 0.145 | 9.74 | 0.000457 | 0.0149 |
| 0.045 | 27.0 | 0.0425 | 0.00181 | 0.150 | 9.42 | 0.000289 | 0.0159 |
| 0.050 | 24.9 | 0.0354 | 0.00211 | 0.155 | 9.12 | 0.000168 | 0.0170 |
| 0.055 | 23.1 | 0.0296 | 0.00244 | 0.160 | 8.84 | $8.50\times10^{-5}$ | 0.0181 |
| 0.060 | 21.5 | 0.0248 | 0.00280 | 0.165 | 8.57 | $3.41\times10^{-5}$ | 0.0193 |
| 0.065 | 20.2 | 0.0208 | 0.00321 | 0.170 | 8.32 | $8.35\times10^{-6}$ | 0.0204 |
| 0.070 | 18.9 | 0.0175 | 0.00366 | 0.175 | 8.08 | $2.86\times10^{-7}$ | 0.0217 |
| 0.075 | 17.9 | 0.0146 | 0.00414 | $1/4\sqrt{2}$ | 8 | 0 | $1/32\sqrt{2}$ |
| 0.080 | 16.9 | 0.0122 | 0.00466 | | | | |

Table 4. Polytrope Expansion Waves.

| $\gamma$ | $x_*$ | $x_{\rm ew}$ | $m_0$ | $m_{\rm ew}$ |
|---|---|---|---|---|
| 0 | 0.0244 | 0.17678 | 0.000667 | 0.022097 |
| 0.1 | 0.0340 | 0.21384 | 0.00156 | 0.039756 |
| 0.2 | 0.0472 | 0.25806 | 0.00356 | 0.070502 |
| 0.3 | 0.0658 | 0.31061 | 0.00797 | 0.12287 |
| 0.4 | 0.0917 | 0.37276 | 0.0175 | 0.20964 |
| 0.5 | 0.128 | 0.44583 | 0.0373 | 0.34835 |
| 0.6 | 0.181 | 0.53111 | 0.0774 | 0.55970 |
| 0.7 | 0.259 | 0.62964 | 0.156 | 0.86089 |
| 0.8 | 0.380 | 0.74183 | 0.301 | 1.24939 |
| 0.9 | 0.585 | 0.86668 | 0.558 | 1.67391 |
| 1 | 1 | 1 | 0.975 | 2 |

**REFERENCES**


Adams, F. C., Lada, C. J., & Shu, F. H. 1987, ApJ, 312, 788

André, P., & Montmerle, T. 1994, ApJ, 420, 837

André, P., Ward-Thompson, D., & Barsony, M. 1993, ApJ, 406, 122

Barsony, M. 1994, in ASP Conf. Ser. 65, Clouds Cores and Low Mass Stars, ed. D. P. Clemens & R. Barvainis (San Francisco: ASP), 197

Bertoldi, F., & McKee, C. F. 1992, ApJ, 395, 140

Bodenheimer, P., & Sweigart, A. 1968, ApJ, 152, 515

Bonnell, I. A., Bate, M. R., & Price, N. M. 1996, MNRAS, 279, 121

Bonnor, W. B. 1956, MNRAS, 116, 351

Bontemps, S., André, P., Tereby, S., & Cabrit, S. 1996, A&A, in press

Boss, A. P., & Black, D. C. 1982, ApJ, 258, 270

Butner, H. M., Evans, N. J., Harvey, P. M., Mundy, L. G., Natta, A., & Randich, M. S. 1990, ApJ, 364, 164

Butner, H. M., Evans, N. J., Lester, D. F., Levreault, R. M., & Strom, S. E. 1991, ApJ, 376, 636

Caselli, P., & Myers, P. C. 1995, ApJ, 446, 665

Chandrasekhar, S. 1967, An Introduction to the Study of Stellar Structure (New York: Dover)

Ebert, R. 1955, ZAp, 37, 217

Elmegreen, B. G. 1989, ApJ, 338, 178

Elmegreen, B. G., & Clemens, C. 1985, ApJ, 294, 523

Foster, P. N., & Chevalier, R. A. 1993, ApJ, 416, 303

Fuller, G. A., & Myers, P. C. 1992, ApJ, 384, 523

Galli, D., & Shu, F. H. 1993a, ApJ, 417, 220

Galli, D., & Shu, F. H. 1993b, ApJ, 417, 243

Goldreich, P., & Weber, S. V. 1980, ApJ, 238, 991

Hills, J. G. 1980, ApJ, 225, 986

Hunter, C. 1977, ApJ, 218, 834

Jijina, J., & Adams, F. C. 1996, ApJ, 462, 874

Kenyon, S. J., Calvet, N., & Hartmann, L. 1993, ApJ, 414, 676

Kenyon, S. J., Gomez, M., Marzke, R. O., & Hartmann, L. 1994, AJ, 108, 251

Kenyon, S. J., Hartmann, L. W., Strom, K. M., & Strom, S. E. 1990, AJ, 99, 869

Lada, C. J., Margulis, M., & Dearborn, D. 1984, ApJ, 285, 141

Larson, R. B. 1969, MNRAS, 145, 271

Larson, R. B. 1981, MNRAS, 194, 809

Lizano, S., & Shu, F. H. 1989, ApJ, 342, 834

Maloney, P. 1988, ApJ, 334, 761

McCrea, W. H. 1957, MNRAS, 117, 562

McKee, C. F. 1989, ApJ, 345, 782

McKee, C. F., & Zweibel, E. G. 1995, ApJ, 440, 686

McLaughlin, D. E., & Pudritz, R. E. 1996, ApJ, 469, in press (MP96)

Myers, P. C., & Benson, P. J. 1983, ApJ, 266, 309

Myers, P. C., & Fuller, G. A. 1992, ApJ, 396, 631

Myers, P. C., & Fuller, G. A. 1993, ApJ, 402, 635

Myers, P. C., & Goodman, A. A. 1988, ApJ, 329, 392

Myers, P. C., Fuller, G. A., Mathieu, R. D., Beichman, C. A., Benson, P. J., Schild, R. E., & Emerson, J. P. 1987, ApJ, 319, 340

Myhill, E. A., & Kaula, W. M. 1992, ApJ, 386, 578

Penston, M. V. 1969, MNRAS, 144, 425

Pudritz, R. E., Wilson, C. D., Carlstrom, J. E., Lay, O. P., Hills, R. E., & Ward-Thompson, D. 1996, ApJ Letters, in press

Shu, F. H. 1977, ApJ, 214, 488

Shu, F. H., Adams, F. C., & Lizano, S. 1987, ARA&A, 25, 23

Suto, Y., & Silk, J. 1988, ApJ, 326, 527

Tereby, S., Shu, F. H., & Cassen, P. 1984, ApJ, 286, 529

Tsai, J. C., & Hsu, J. J. L. 1995, ApJ, 448, 774

Whitworth, A., & Summers, D. 1985, MNRAS, 214, 1

Zhou, S. 1992, ApJ, 394, 204

Zhou, S., Evans, N. J., Kömpe, C., & Walmsley, C. M. 1993, ApJ, 404, 232

Zhou, S., Evans, N. J., Butner, H. M., Kutner, M. L., Leung, C. M., & Mundy, L. G. 1990, ApJ, 363, 168

---

This preprint was prepared with the AAS LaTeX macros v4.0.

Fig. 1.— Density profiles of a pressure-truncated logotrope and the Bonnor-Ebert isothermal sphere. Both configurations are in hydrostatic equilibrium, and correspond to critical-mass clouds, i.e., an increased central concentration in either case would destabilize the equilibrium. The scale radius is $r_0 = 3\sigma_c/(4\pi G\rho_c)^{1/2}$, and $\rho_s$ is the density at the cloud surface. The broken lines trace the singular profiles for each equation of state; note how such a solution mirrors the true behavior of the logotrope at most $r$, but bears little resemblance to any stable isothermal sphere.

Fig. 2.— Velocity fields for various logotrope collapse solutions. Solid curves are minus solutions, and broken lines are plus solutions; the dash-dot line traces the locus of critical points. The heavy solid line represents the expansion wave, which continues to $x = \infty$ with $v \equiv 0$ and densities given by the hydrostatic singular solution. The minus solutions to the left of the expansion wave reach $v = 0$ at some finite $x$, and therefore have vanishingly small spatial extent at $t = 0$. The minus solutions to the right of the expansion wave follow the collapse of spheres which are initially out of hydrostatic equilibrium. The expansion wave is the limit of both sequences.

Fig. 3.— Density profile and velocity field, in similarity variables, of the expansion-wave solution for a collapsing logotrope. The heavy black lines trace out the region of dynamical collapse inside the expansion wave, like the same line type in Fig. 2, while the thin solid line in the top panel is the hydrostatic singular solution $\alpha = 2^{1/2}/x$. The dashed lines are the expected free-fall solutions $\alpha \sim x^{-3/2}$ and $v \sim x^{-1/2}$. Vertical (dotted) lines show the time-dependent location $X = R/a_t t$ of the cloud's outer radius.

Fig. 4.— Expansion-wave accretion timescales for stars in an $A = 0.2$ logotrope and a singular, $T = 10$ K isothermal sphere. Low-mass stars take longer to form in the logotrope, while more massive ones accrete more rapidly.

Fig. 5.— Time evolution (from left to right), in dimensional variables, of the density profile and velocity field for a collapsing logotrope of $1M_\odot$ with a kinetic temperature $T = 10$ K and under a surface pressure $P_s = 1.3 \times 10^5\ k\ \mathrm{cm}^{-3}$ K. The solid curves lie in the interior of the expansion wave (and therefore correspond to the heavy black lines in Figs. 2 and 3), and the broken line in the top panel traces the hydrostatic $r^{-1}$ density profile out to the boundary $R$ of the initial cloud. The times shown are roughly the same $t/\bar{t}_{\rm ff}$ used to locate $X$ in Fig. 3.

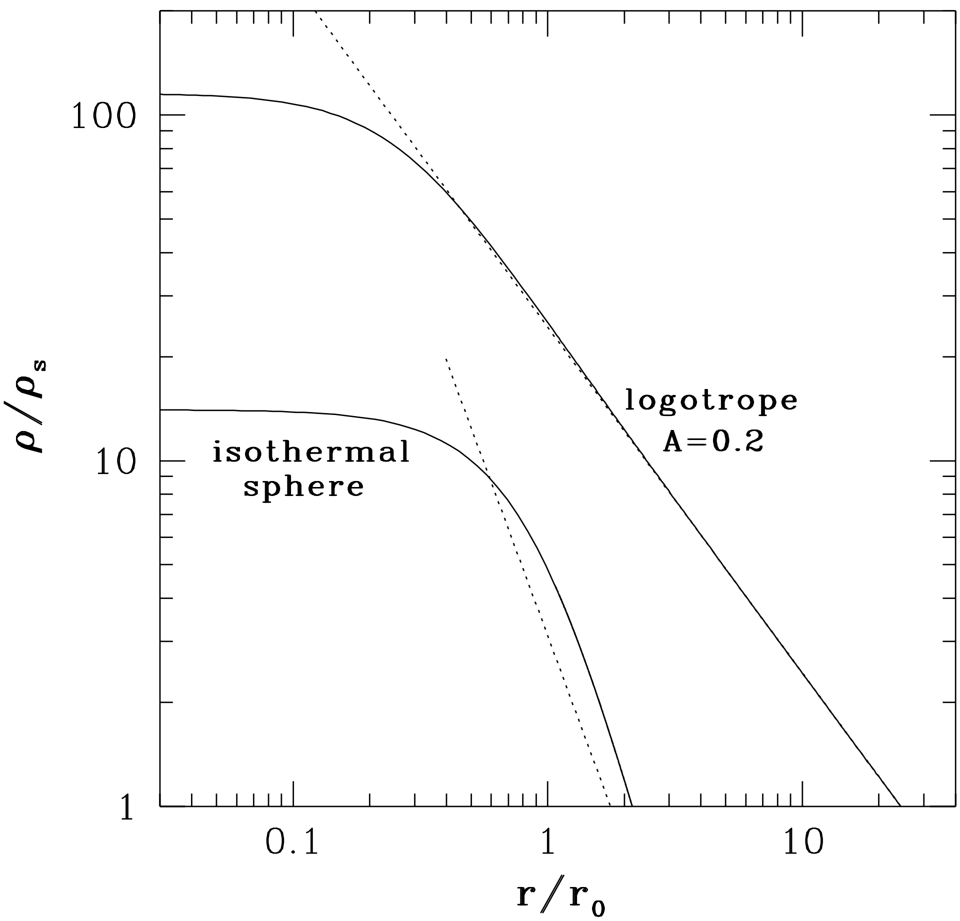
100
10
1
0.1
1
10
$\rho/\rho_s$
$r/r_0$
logotrope
A=0.2
isothermal
sphere

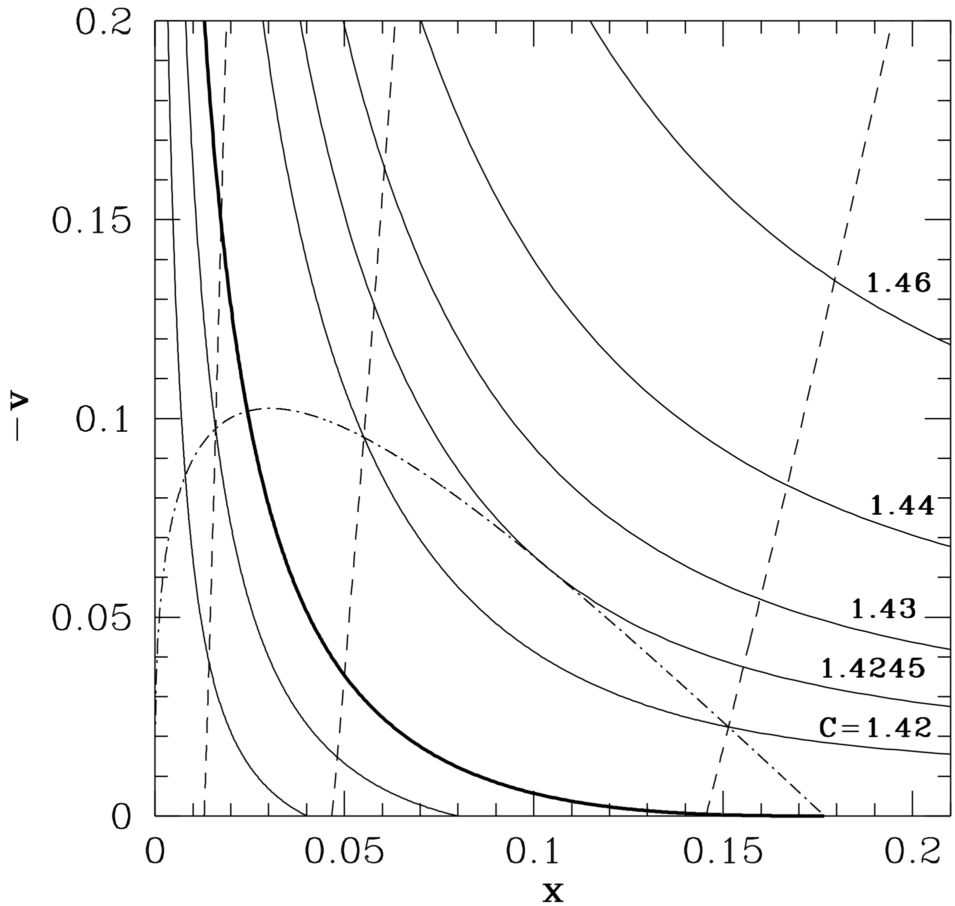

0.2
0.15
0.1
0.05
0
−v
0
0.05
0.1
0.15
0.2
x
1.46
1.44
1.43
1.4245
C=1.42

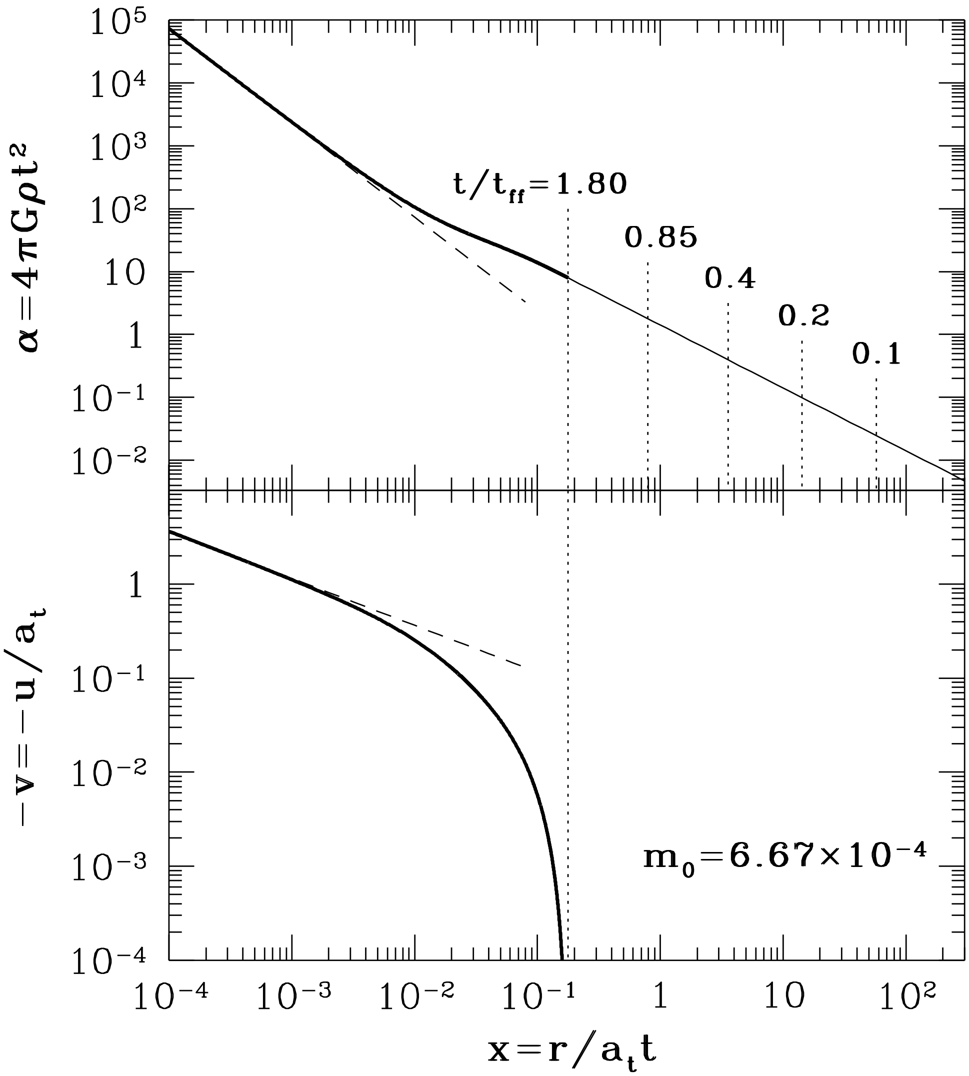

$\alpha = 4\pi G \rho t^2$
$t/t_{ff} = 1.80$
0.85
0.4
0.2
0.1
$-v = -u/a_t$
$m_0 = 6.67 \times 10^{-4}$
$x = r/a_t t$

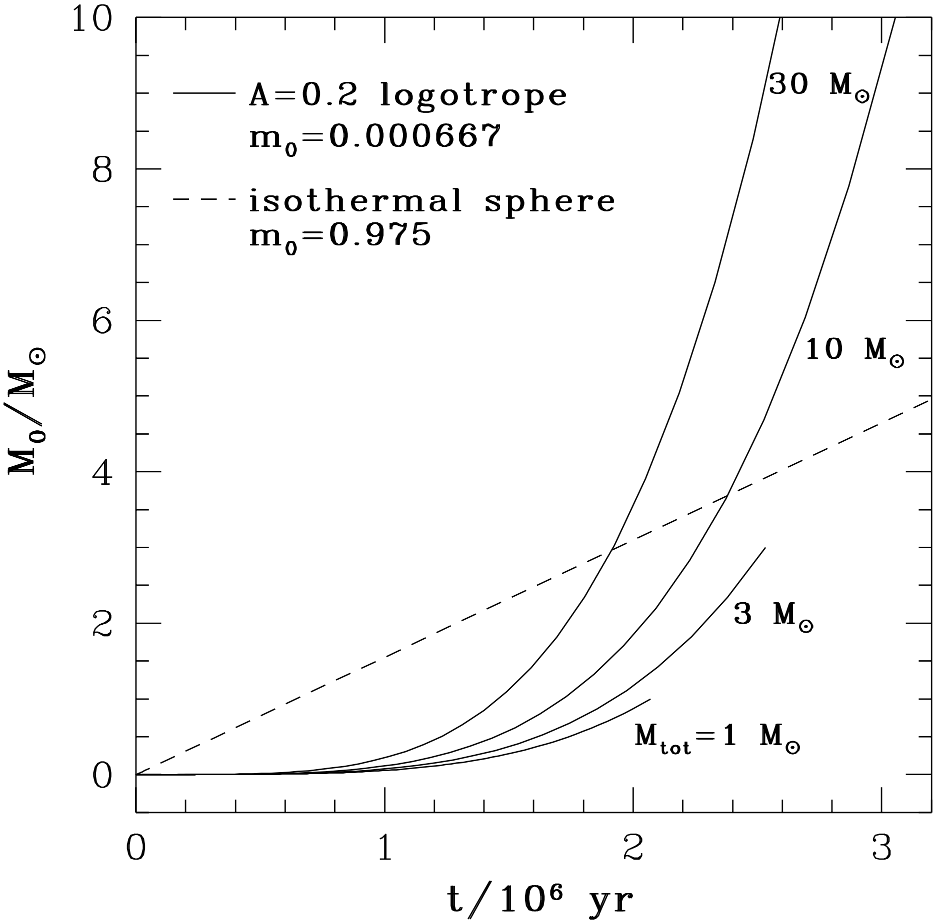
A=0.2 logotrope
m0=0.000667
isothermal sphere
m0=0.975
30 M⊙
10 M⊙
3 M⊙
Mtot=1 M⊙
M0/M⊙
t/10⁶ yr
0
2
4
6
8
10
0
1
2
3

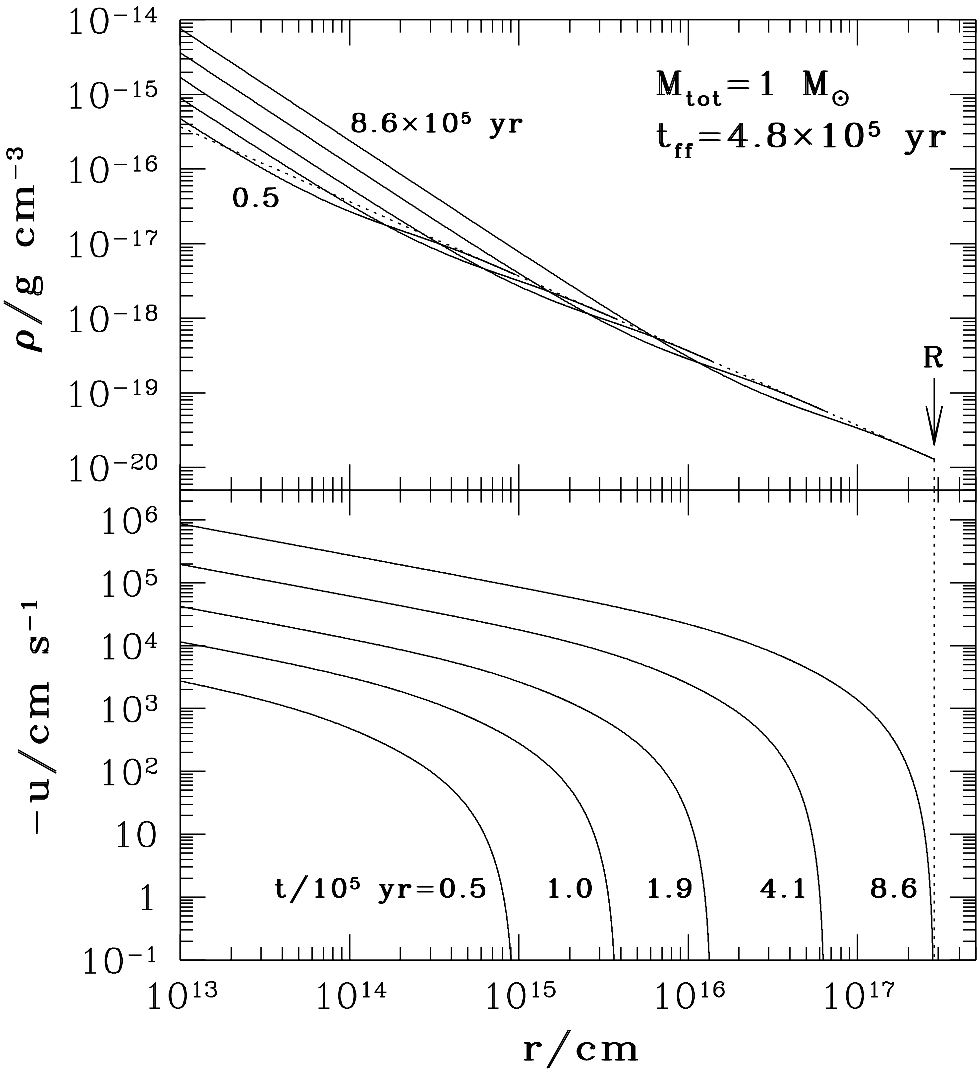

$M_{tot}=1\ M_\odot$
$t_{ff}=4.8\times10^5$ yr
$8.6\times10^5$ yr
0.5
R
$\rho$/g cm$^{-3}$
$-u$/cm s$^{-1}$
$t/10^5$ yr=0.5
1.0
1.9
4.1
8.6
r/cm